

LIBRARY

MR No. L6H14

19 MAR 1948

NATIONAL ADVISORY COMMITTEE FOR AERONAUTICS

# WARTIME REPORT

ORIGINALLY ISSUED

August 1946 as  
Memorandum Report L6H14

AN EXPERIMENTAL INVESTIGATION OF FLOW

CONDITIONS IN THE VICINITY OF AN

NACA D<sub>8</sub>-TYPE COWLING

By Robert W. Boswinkle, Jr., and Rosemary P. Bryant

Langley Memorial Aeronautical Laboratory  
Langley Field, Va.

# NACA

WASHINGTON

N A C A LIBRARY  
LANGLEY MEMORIAL AERONAUTICAL  
LABORATORY  
Langley Field, Va.

NACA WARTIME REPORTS are reprints of papers originally issued to provide rapid distribution of advance research results to an authorized group requiring them for the war effort. They were previously held under a security status but are now unclassified. Some of these reports were not technically edited. All have been reproduced without change in order to expedite general distribution.



3 1176 01403 6041

## NACA LANGLEY MEMORIAL AERONAUTICAL LABORATORY

## MEMORANDUM REPORT

MR No. L6H14

## AN EXPERIMENTAL INVESTIGATION OF FLOW

## CONDITIONS IN THE VICINITY OF AN

NACA D<sub>8</sub>-TYPE COWLING

By Robert W. Boswinkle, Jr., and Rosemary P. Bryant

## SUMMARY

An investigation has been conducted in the Langley 20-foot propeller-research tunnel to determine the flow conditions in the vicinity of an NACA D<sub>8</sub>-type cowling. A 1/2-scale-nacelle model was used for the tests. Data were obtained for inlet-velocity ratios ranging from 0.23 to 1.02 and for angles of attack from 0° to 10°.

With the propeller removed, the speeds and directions of the flow in the vertical plane of symmetry of the cowling were determined from orifices and tufts installed on a board aligned with the flow. The total pressures and the rotation of the flow at the inlet were determined for two propellers having greatly different shank sections. Oval fairings were glued to the root sections of one propeller in order to simulate poorly designed blade shanks. An NACA 16-series propeller with thin airfoil-type inboard sections was used to simulate well designed blade shanks. Tests were conducted at advance-diameter ratios and propeller-blade angles, both based on the maximum spinner diameter, ranging from about 2.5 to 15.5 and from 37.5° to 62.5°, respectively.

The local airspeeds and flow directions were found to have appreciable gradients in the region of the propeller shanks. The propeller with thin airfoil-type shanks caused higher total pressures and larger angles of flow rotation at the cowling inlet for the high-speed and climb flight conditions than the propeller with thick oval shanks. At a constant blade-shank angle, the changes of flow rotation and total-pressure rise caused by changes in advance-diameter ratio were smaller for the propeller with thick oval shanks

than for the propeller with thin airfoil-type shanks over the complete operating range of inlet-velocity ratio. The magnitude of the changes in the flow rotation in the inlet was such that, in order to secure effective operation over the flight range, contravanes would be required upstream of a fan installed in the inlet of this cowling.

## INTRODUCTION

A large amount of research effort is being directed currently toward the development of efficient propeller-blade shanks and high-pressure-rise cooling fans for use in conjunction with conventional radial-engine cowlings. The design of these elements, however, is still largely on a cut-and-try basis despite the numerous advances in propeller and fan theory because of the lack of information on the actual flow conditions under which they operate. As a step toward the rational solution of this problem, the present investigation of a 1/2-scale NACA D<sub>8</sub>-type cowling was conducted in the Langley 20-foot propeller-research tunnel to obtain initial quantitative design information.

Wide operating ranges of inlet-velocity ratio and angle of attack were covered in the tests. With the propeller removed, the speeds and the directions of the flow in the vicinity of the cowling were determined. The total pressure and rotation of the flow in the inlet were investigated over wide ranges of propeller-shank blade-angle and propeller-shank advance-diameter ratio for a propeller having thick oval shank sections and a propeller having thin airfoil-type shank sections. Some similar data for a Hercules Beaufighter nacelle equipped alternately with a flared propeller and spinner and with an unflared propeller are contained in reference 1.

## SYMBOLS

$D_c$	maximum cowling diameter, 2.27 feet
$D_s$	maximum spinner diameter, 1.42 feet
$H$	total pressure, pounds per square foot
$\Delta H/q_f$	pressure-drop coefficient for orifice plate based on maximum cross-sectional area of cowling
$n$	rotational speed, revolutions per second

$p_o$	free-stream static pressure, pounds per square foot
$q_o$	free-stream dynamic pressure, pounds per square foot
$r$	radius, feet
$R$	radius of propeller tip, feet
$V_i$	inlet velocity, feet per second
$V_l$	local speed of flow, feet per second
$V_o$	free-stream velocity, feet per second
$\alpha$	angle of attack of thrust axis, degrees
$\beta_s$	propeller-blade angle at station corresponding to maximum spinner diameter, degrees
$\delta$	cowling-flap angle from flush position, degrees
$\theta$	clockwise angle around cowling from bottom as seen from the front, degrees
$\phi$	flow angle referred to model center line (positive upward), degrees
$\psi$	angle of flow rotation (positive in direction of propeller rotation), degrees

#### MODEL AND METHODS

A 1/2-scale model of a nacelle for a present-day short-nose radial engine was used for the tests. A line drawing of the model and coordinates of the spinner, diffuser, and cowling are presented in figure 1. The cowling had an inlet area of 0.71 square foot and a critical Mach number of 0.63 at an angle of attack of  $0^\circ$  and an inlet-velocity ratio of 0.23.

The internal flow was measured by an orifice plate to which mockups of the forward halves of the front-row cylinders were attached. The effective orifice area was adjusted to 0.70 square foot ( $\Delta h/q_f = 33.6$ ) in a calibration prior to the tunnel tests in order that the conductivity would approximate that encountered in modern engine installation. The rate of flow through the cowling

was varied by the use of alternate exit flaps with different angular deflections. Test inlet-velocity ratios ranged between 0.23 and 1.02.

The orifice board used in determining the local speeds and directions of flow in the vertical plane of symmetry of the cowl with the propeller removed is shown in general views of the model. (See fig. 2.) The board was 0.5-inch thick and had lenticular edges. Local flow speeds were determined from the static pressures measured by the flush surface orifices on the left side of the board; pressure measurements on the surfaces of the cowl and the spinner with the orifice board removed furnished a convenient check on the speeds just outside the boundary layers. The direction of the flow was determined from photographs of the tufts fastened to the right side of the board; check runs with tufts on wires showed that there were no measurable differences in the flow angles inside and outside the boundary layer of the orifice board.

As shown in the detail views of the cowl (fig. 3) two alternate left-hand propellers were used. Oval-shank fairings were glued to the blades of the 45-inch-diameter Curtiss 512 propeller in the top configuration in order to simulate a propeller with poorly designed shank sections. A 49.3-inch-diameter Curtiss 1129-24 (NACA 16-series) propeller with thin-airfoil-type shank sections was used in the bottom configuration. The shank sections of these two propellers (figs. 4, 5, and 6) bracketed the range of shank designs in current use. The propellers were driven by a 100-horsepower alternating-current motor; the propeller rotational speed was measured by a condenser-type tachometer attached to the motor shaft.

Total pressures in the boundary layer of the spinner at the inlet were measured by a rake of ten 0.030-inch-diameter stainless-steel tubes with ends flattened to form openings about 0.005 by 0.05 inch. The average pressure recoveries in the inlet were determined from the arithmetic average of the total pressures measured by eight pairs of shielded total-pressure tubes spaced  $45^\circ$  apart starting at the bottom of the inlet. For the propeller-installed tests, the boundary-layer rake and all shielded total-pressure tubes excepting those at  $45^\circ$ ,  $90^\circ$ , and  $135^\circ$  from the bottom on the left side were removed to permit the installation of the other instrumentation (see fig. 3); pressure recoveries for the diametrically opposite positions on the right side of the inlet were obtained for propeller-installed conditions by the expedient of testing at negative angles of attack.

Null-calibrated yaw tubes (fig. 7(a)) were placed in the inlet at  $0^\circ$ ,  $45^\circ$ ,  $90^\circ$ , and  $135^\circ$  from the bottom on the right side to measure the flow rotation. The yaw-tube settings were varied in increments of  $5^\circ$  for each operating condition until the differential pressure across the two legs reversed; the angle of flow rotation corresponding to the zero pressure difference was then determined by fairing the pressure differential against the tube setting. As the angles of rotation indicated by the inner and outer tubes were approximately equal and exhibited no consistent variation, an average value was taken as the flow rotation at each radial position. As with the shielded total-pressure tubes, the flow rotation at the diametrically opposite inlet positions were obtained by testing at negative angles of attack.

In an attempt to check on the values of rotation given by the yaw tubes, floating vanes were mounted on a wire at the top of the inlet. (See fig. 7(b).) A gun-sight camera mounted behind the orifice plate was used to record the vane deflections which were used to calculate the angularity of the flow.

All tests were conducted at a tunnel speed of about 100 miles per hour which corresponds to a Mach number of 0.13 and a Reynolds number of about 2,000,000 based on the maximum cowling diameter. An angle-of-attack range of from  $0^\circ$  to  $10^\circ$  was covered in the tests; the latter angle is approximately equal to the effective steep-climb angle of attack for a cowling operating in the up-flow field of a wing. All pressures excepting those for the yaw tubes were recorded by photographing a multitube manometer. The differential pressures across the yaw tubes were read visually from a bank of inclined U-tube manometers.

## RESULTS AND DISCUSSION

The results of the present investigation are discussed in three sections which deal separately with the flow field of the cowling, the pressure recovery in the cowling inlet, and the rotation of the flow in the cowling inlet.

Flow field of cowling.- Velocity-ratio contours and lines of constant flow angle are shown in figure 8 for the several test conditions. The local airspeeds and flow directions are shown to have appreciable gradients in the region in which the propeller shanks would normally operate. At constant inlet-velocity ratios, the local airspeeds in the propeller-shank region at the top of the spinner increased and those at the bottom decreased with

increases in the angle of attack; the local angles of upflow increased in both regions. As would be expected, increasing the inlet-velocity ratio at constant angles of attack caused increases in the local airspeeds and decreases in the magnitudes of the local flow angles in the propeller-shank region.

It should be noted that in figure 8 that  $V_1/V_0$  is a scalar quantity; therefore, the translational velocity ratio (that is, the velocity ratio at a point in the inlet  $V_1/V_0$ ) is  $(V_1/V_0) \cos \phi$ . The high values of  $\phi$  at the inlet together with the rapid thickening of the boundary layer in this vicinity accounts for the large apparent differences at low inlet-velocity ratios between the nominal inlet-velocity ratio and the  $V_1/V_0$  contours adjacent to the inlet. It also should be noted that the lines of constant-velocity ratio are true contours and form closed curves in the plane of the orifice board while the lines of constant flow angle do not necessarily close in this plane and may end at the surface of the model or at a point in space.

As previously noted, the present data were obtained at a Mach number of 0.13. Some change in the flow-field characteristics would be expected at very high flight speeds, but the changes would be small up to  $M_0 = 0.63$ , the design Mach number for this installation.

Pressure recovery at cowling inlet.- Total-pressure distributions in the boundary layer at the top of the spinner for propeller-removed conditions are shown in figure 9. With the spinner stationary (fig. 9(a)) the boundary layer was thin for an inlet-velocity ratio of about 0.83. The occurrence of separation from the surface at  $V_1/V_0 \approx 0.23$ , as evidenced by the tendency of the total pressures to remain equal to the surface-static pressures (plotted at the surface) for 0.2 inch or more from the surface, indicates that a somewhat higher inlet-velocity ratio should be used. This effect has been observed in several previous investigations in which minimum values of  $V_1/V_0$  ranging from 0.3 to 0.5 have proved necessary. Figure 9(b) shows that at  $V_1/V_0 \approx 0.83$ , rotation of the spinner thickened the boundary layer somewhat but did not cause separation. Propeller operation would be expected to cause additional thickening of the boundary layer at the inlet.

The circumferential variation of the average pressures measured by the pairs of shielded total-pressure tubes for propeller-removed conditions are shown in figure 10. At inlet-velocity ratios of approximately 0.68 and 0.84, nearly 100-percent recovery

was measured at all stations. At  $V_1/V_0 = 0.23$  and  $\alpha = 0^\circ$  appreciable losses occurred due to the boundary-layer characteristics previously discussed; increasing the angle of attack to  $10^\circ$  greatly accentuated these separation losses at the top of the inlet.

At  $\alpha = 10^\circ$  with the propeller operating, the total pressures at six circumferential positions in the inlet, as determined from the shielded total-pressure tube instrumentation, are shown in figure 11 as a function of  $V_0/nD_s$ ,  $\delta$ , and  $\beta_s$ . As would be expected from a consideration of the swirl of the flow and the attitudes of the propeller-blade elements, the highest and lowest total pressures occurred in the bottom-left and top-right portions of the inlet, respectively. The total pressure at any one position generally decreased with increases in  $V_0/nD_s$  and decreases in  $\beta_s$  as the effective angle of attack of the shank elements was reduced. The inlet-velocity ratios for figure 11 and succeeding figures showing plots at constant values of flap angle may be obtained by reference to figure 12.

The arithmetic averages of the inlet total pressures are plotted in figure 13 as a function of the same parameters used in the preceding figure. Because of differences in the camber, the fineness ratio, and the chord of the blade shanks, the propeller with the NACA 16-series shank sections produced higher inlet pressures than the oval-shanked propeller for low values of  $V_0/nD_s$  at  $\delta = 20^\circ$ , a condition corresponding to the climb condition, and for high values of  $V_0/nD_s$  at  $\delta = 0^\circ$ , a condition corresponding to the high-speed condition, over a wide enough range of  $\beta_s$  to include these two flight conditions. A regrouping of the curves for  $\delta = 20^\circ$  (fig. 14) shows that for the climb inlet-velocity ratio the NACA 16-series shank section:

(a) Gave a higher pressure rise than the oval-shank sections over a wide range of blade angle at climb values of  $V_0/nD_s$ .

(b) Apparently did not experience an abrupt stall even at the low values of  $V_0/nD_s$  at which calculations indicate the geometric angle of attack was very large.

(c) Apparently were producing negative thrust at high values of  $V_0/nD_s$ .

A cross plot of the inlet-pressure-recovery data for  $\beta_s = 62.5^\circ$  against  $V_1/V_0$  is presented in figure 15. The pressure recovery increased with  $V_1/V_0$  over most of the  $V_1/V_0$  range

although a uniform decrease would be expected on the basis of propeller theory except at the lower values of  $V_0/nD_S$  where calculations indicate that the shanks probably were stalled and operating on the reverse slopes of the section lift curves. It should be noted, however, that the theoretical decreases

of  $\frac{H - p_0}{q_0}$  with increases of  $V_1/V_0$  would be expected to be

small because the local velocities at the propeller-shank position exhibited only relatively small variations with large changes in  $V_1/V_0$ . (See fig. 8.) Also the shapes of these curves in the lower inlet-velocity-ratio range are not accurately known because each curve was obtained by cross-plotting data measured at only three values of inlet-velocity ratio (about 0.23, 0.70, and 0.86). Figure 10 indicates that the boundary layer on the spinner was responsible to a large extent for the low pressure recoveries measured in the inlet at low inlet-velocity ratios with propeller removed. Spinner boundary-layer effects may also be a factor in the apparent discrepancy between the calculated and measured inlet total-pressure recoveries.

Rotation of flow in inlet.— A comparison of the flow rotation at the top of the inlet as indicated by the yaw tubes and by the vanes is given in figure 16. It should be noted that, in general, fair agreement was obtained between the two sets of readings, but that the readings of the yaw tubes were more consistent than the readings of the vanes. For this reason, and since yaw tubes have given satisfactory results in other investigations, the succeeding analysis of the flow-rotation data is based on the measurements obtained by the yaw tubes only.

The flow rotation in the cowl inlet for propeller-removed conditions is shown in figure 17 as a function of circumferential position, angle of attack, and inlet-velocity ratio. The scatter at  $\alpha = 0^\circ$  indicates that the probable accuracy of the yaw-tube readings was about  $\pm 1.5^\circ$ . The sine-wave type variation at  $\alpha = 10^\circ$  was caused by the upflow at the sides of the inlet. Increasing the inlet -velocity ratio at  $\alpha = 10^\circ$  reduced the rotation at the sides of the inlet by increasing the axial component in the velocity vector diagram.

The flow rotation in the cowl inlet for the propeller-installed conditions is shown in figures 18 and 19 as a function of  $V_0/nD_S$ ,  $\delta$ , and  $\beta_S$  for the two propellers tested. The plots for the average values at  $\alpha = 0^\circ$  (figs. 18(a) and 19(a)) show that the flow rotation with the NACA 16-series propeller became greater than that for the oval-shanked propeller at low

values of  $V_0/nD_s$  and at small flap angles as was the case with the inlet pressures. The occurrence of negative rotation angles indicates the existence of negative thrust thereby confirming the previous deduction based on the variation of the inlet total pressures. A higher shank blade angle than  $62.5^\circ$  would appear desirable for this condition.

At  $\alpha = 10^\circ$  (figs. 18(b) and 18(c)) the maximum positive rotation usually occurred at the right side where the upflow due to angle of attack was a maximum and was additive with the rotation caused by the propeller except at negative thrust. Conversely, the minimum flow rotation usually occurred at the left side where the upflow due to the cowling angle of attack generally opposed the rotation caused by the propeller. For a representative climb condition ( $\alpha = 10^\circ$ ,  $\delta = 20^\circ$ ,  $\beta_s = 50^\circ$ ,  $V_0/nD_s = 3$ ), figure 19(b) shows that maximum and minimum angles of flow rotation in the inlet were about  $22^\circ$  and  $-3^\circ$ , respectively, for the NACA 16-series propeller compared to about  $21.5^\circ$  and  $-5.5^\circ$  for the oval-shanked propeller.

The flow-rotation data for  $\beta_s = 62.5^\circ$  shown in figures 18 and 19 is cross-plotted in figure 20 to show the effect of inlet-velocity ratio. As would be expected, increasing  $V_i/V_0$  tended to decrease the rotation except where the blade-shank elements were operating near the region of negative thrust. The change of flow rotation with changes in  $V_0/nD_s$  was smaller for the oval-shanked propeller than for the NACA 16-series propeller over the complete range of  $V_i/V_0$ ; a comparable result for the inlet total pressure is noted in figure 15.

The data presented in figures 18 through 20 cover a sufficient range of operational variables to permit a fair approximation of the prerotation encountered by a fan in the inlet of a cowling of approximately the proportions tested. The magnitude of the variation of  $\psi$  through the normal-operating ranges stresses the necessity for using contravanes upstream of the fan in order to secure effective operation over the flight range.

#### SUMMARY OF RESULTS

The results of this investigation indicate that:

1. The local airspeeds and flow directions had appreciable gradients in the region of the propeller shanks.

2. The propeller with thin airfoil-type shanks caused higher total pressures and larger angles of flow rotation at the cowling inlet for the high-speed and climb flight conditions than the propeller with thick oval shanks.

3. At a constant blade-shank angle, the changes of flow rotation and total-pressure rise caused by changes in advance-diameter ratio were smaller for the propeller with thick oval shanks than for the propeller with thin airfoil-type shanks for the complete operating range of inlet-velocity ratio.

4. The magnitude of the change of flow rotation in the inlet was such that contravanes would be required upstream of a fan installed in the inlet of this cowling.

Langley Memorial Aeronautical Laboratory  
National Advisory Committee for Aeronautics  
Langley Field, Va.

#### REFERENCE

1. Nicholson, L. F., and Shaw, H.: 24-Foot Tunnel Tests on the Cowl Entry Losses on a Hercules Beaufighter Nacelle Fitted with Flared and Unflared Propellers. Rep. No. Aero 2047, British R.A.E., May 1945.

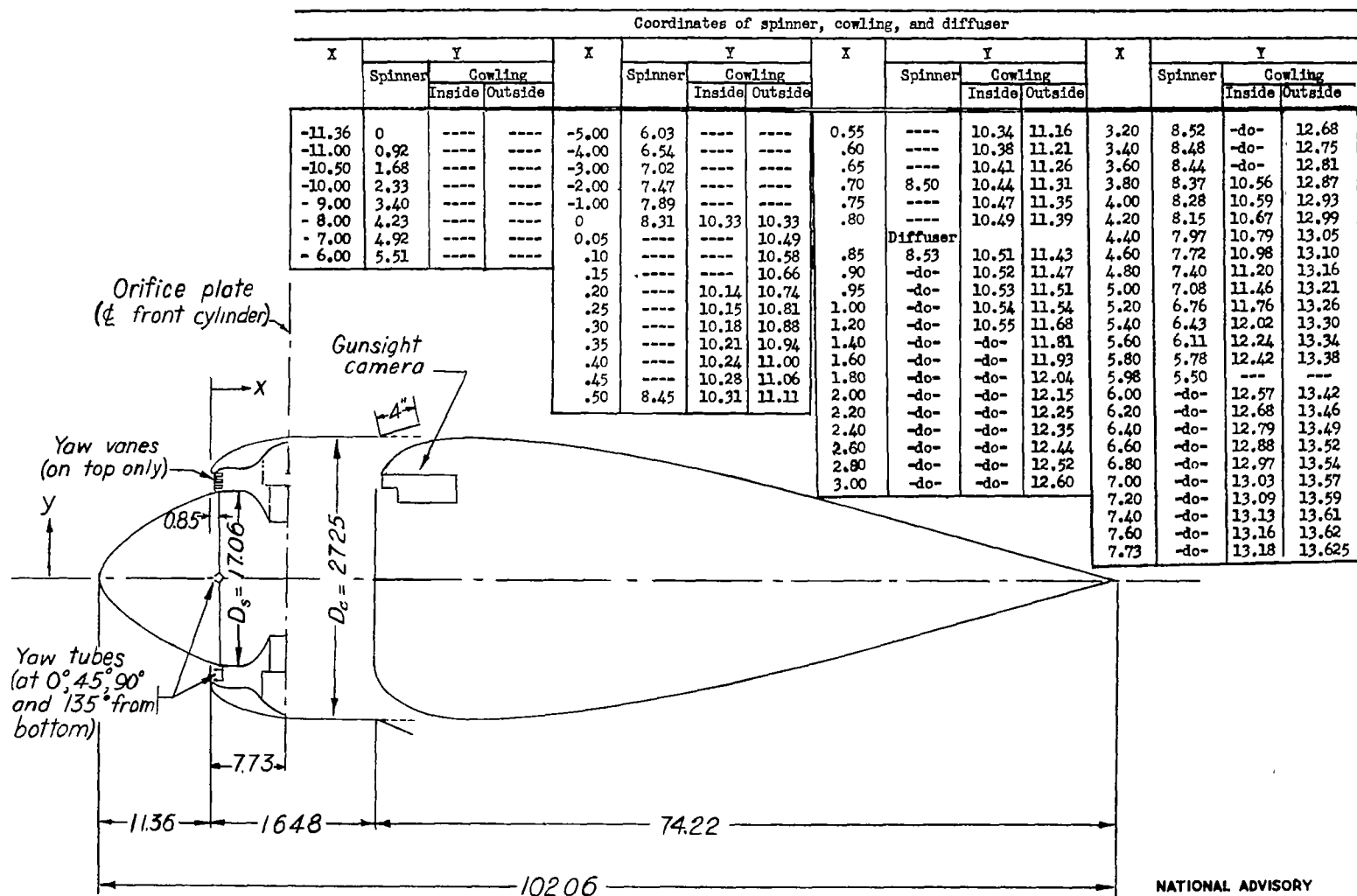
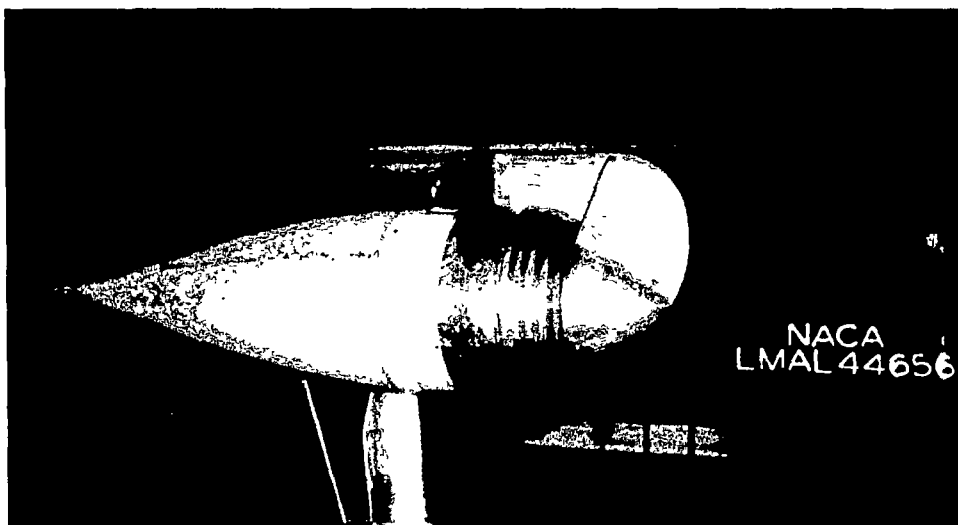
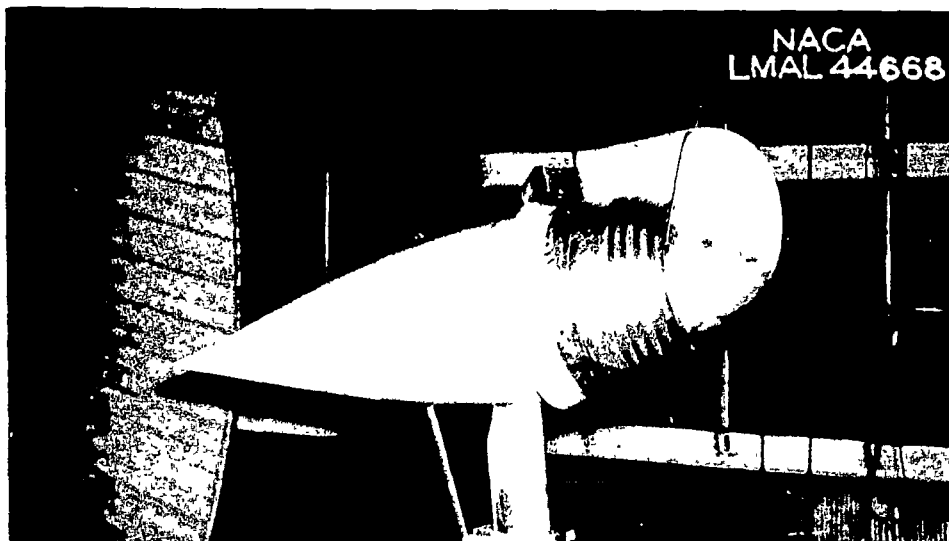


Figure 1.—General arrangement and principal dimensions of model All dimensions in inches.

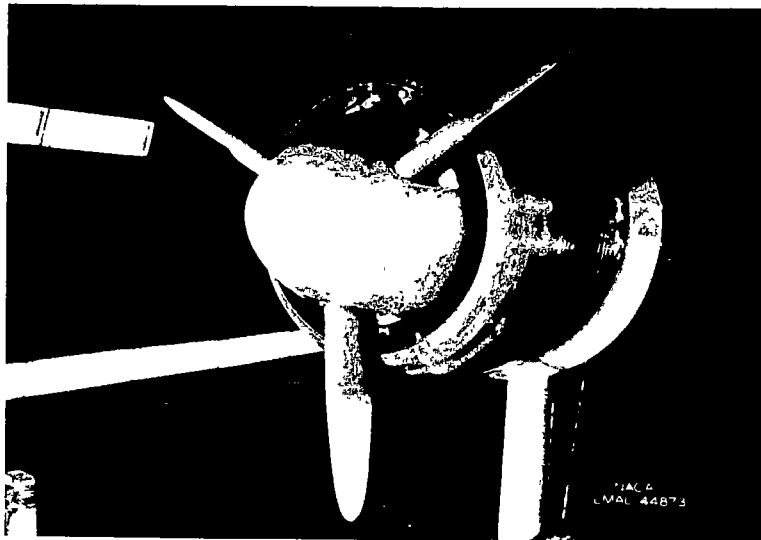


$$(a) \alpha = 0, \delta = 0, \frac{V_i}{V_o} = 0.23.$$



$$(b) \alpha = 10, \delta = 20, \frac{V_i}{V_o} = 0.81.$$

Figure 2.- General views of model with orifice board installed.

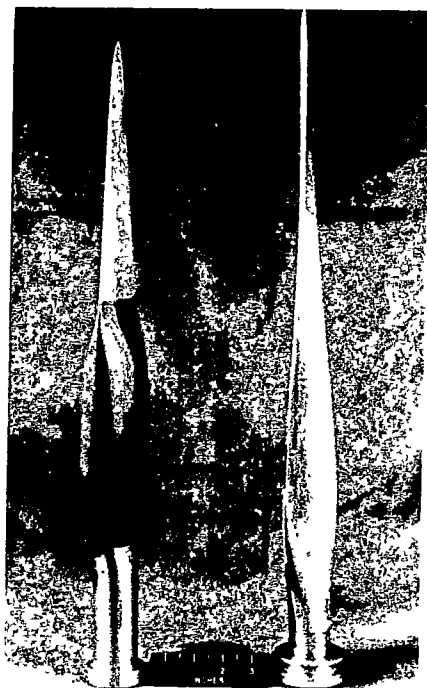


(a) Oval-shanked propeller installed.



(b) NACA 16-series propeller installed.

Figure 3.- General views of cowling showing the two propeller configurations.



Curtiss 1129-24  
NACA 16-series  
blade

Curtiss 512 blade  
with oval-shank  
fairing

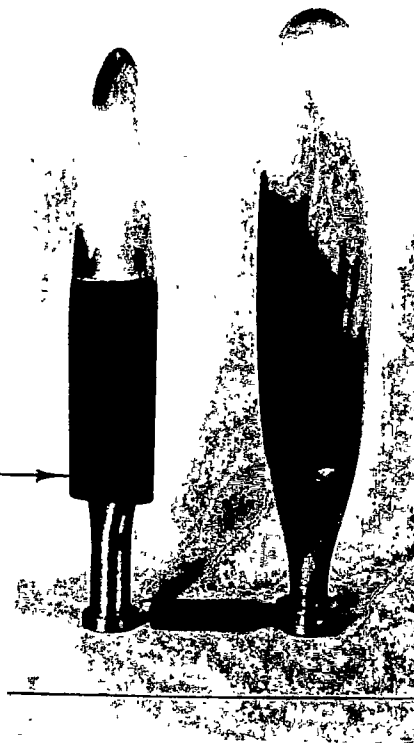


Figure 4.- Detail views of propeller blades.

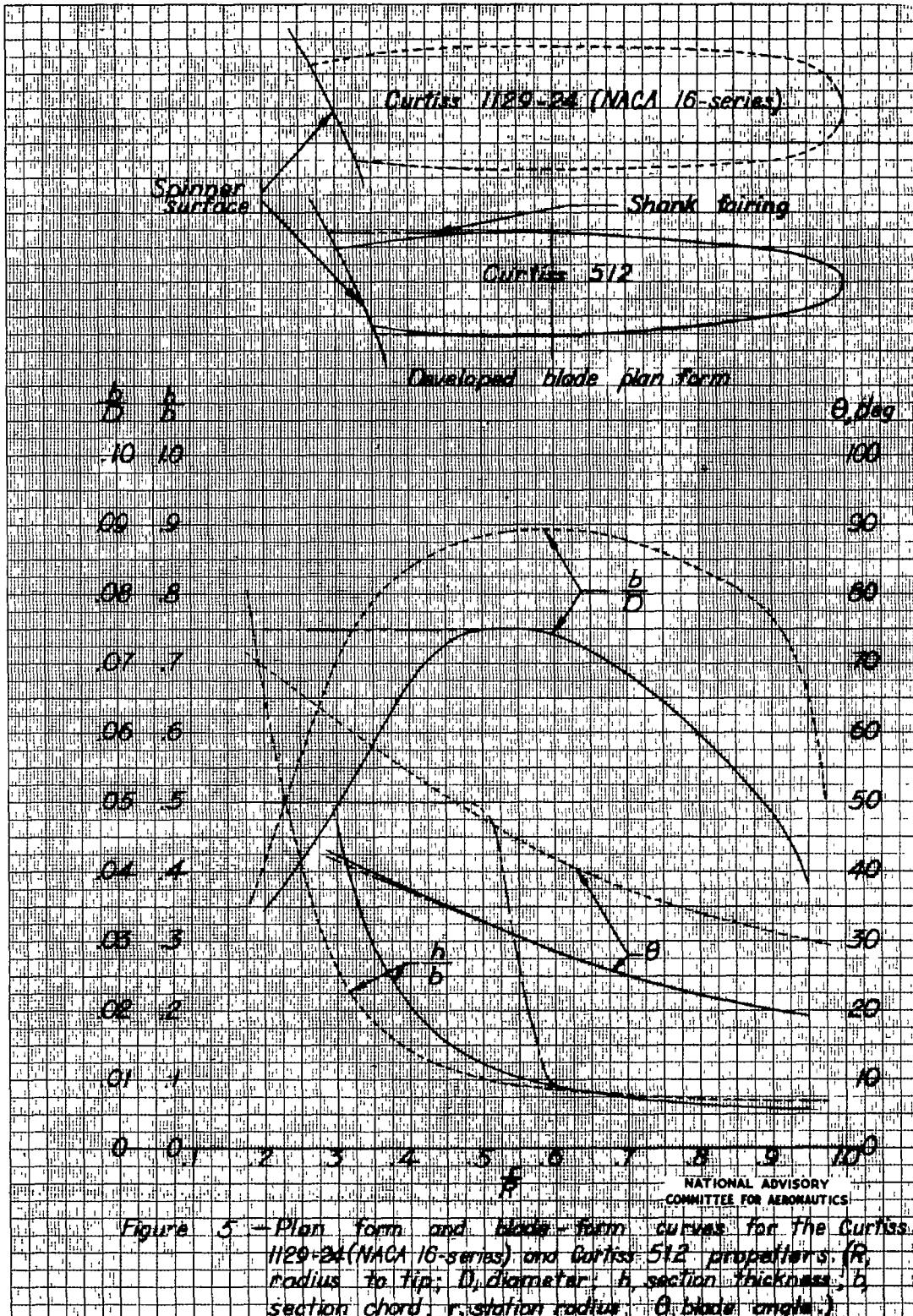
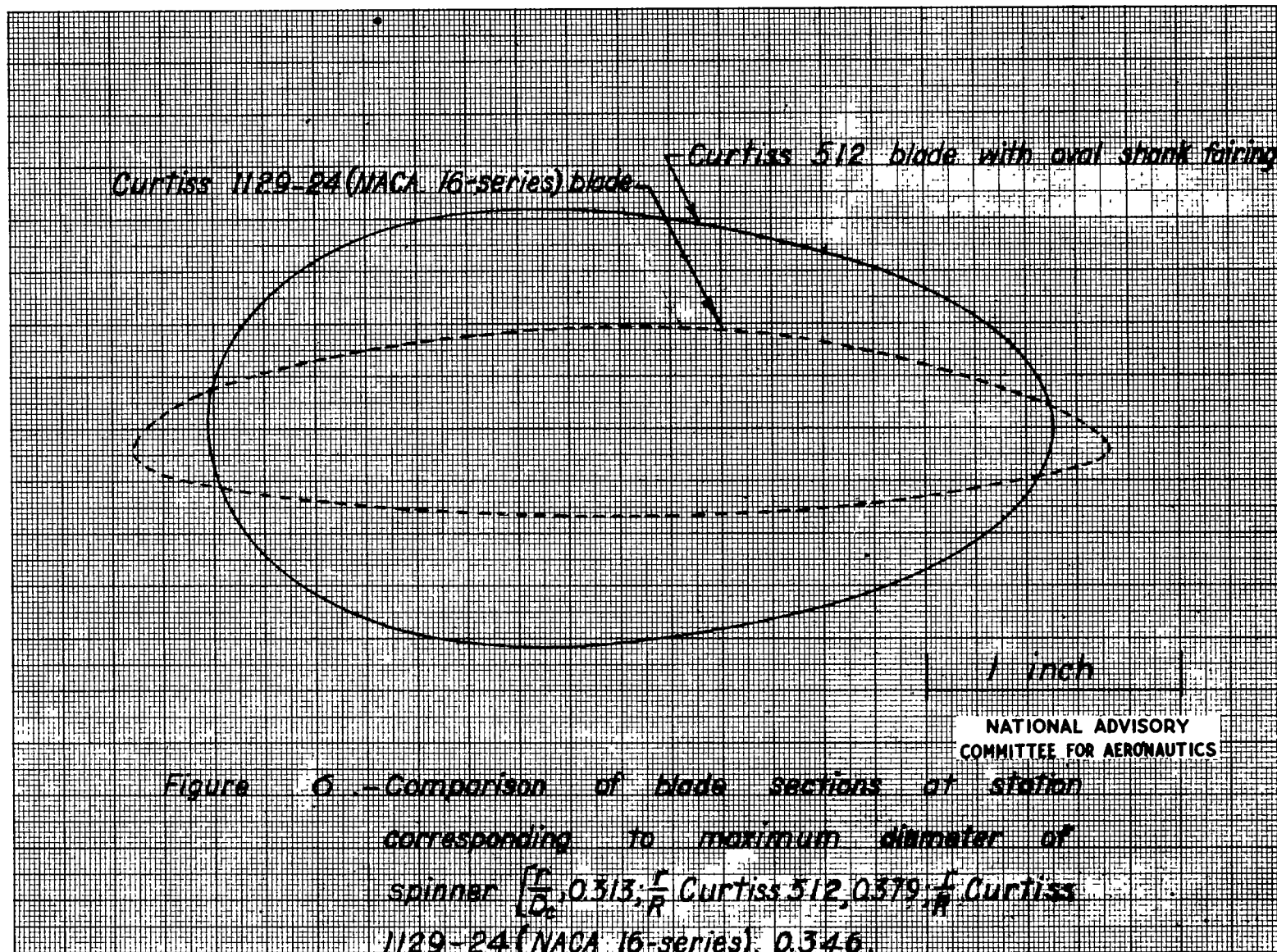
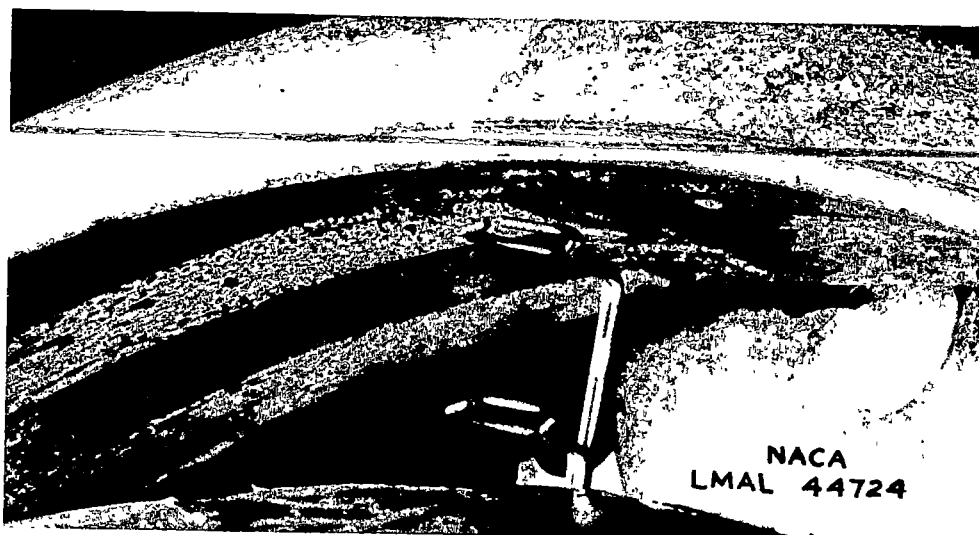


Figure 5 - Plan form and blade-form curves for the Curtiss 1129-24 (NACA 16-series) and Curtiss 512 propellers. ( $R$ , radius to tip;  $D$ , diameter;  $h$ , section thickness;  $b$ , section chord;  $r$ , station radius;  $\theta$ , blade angle.)



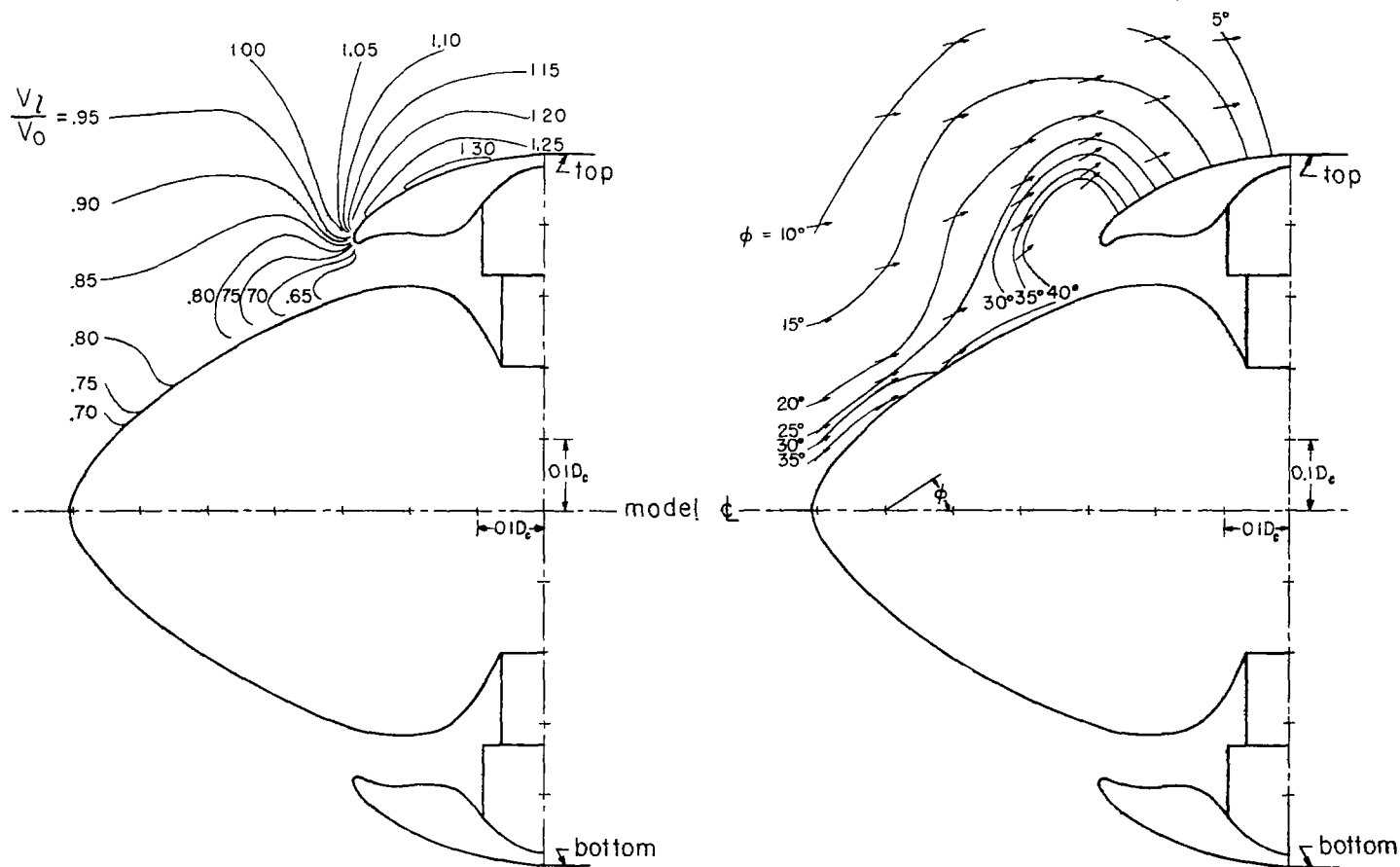


(a) Typical pair of yaw tubes.



(b) Vanes at top of cowling.

Figure 7.- Views of instrumentation used to measure rotation of flow in cowling inlet.

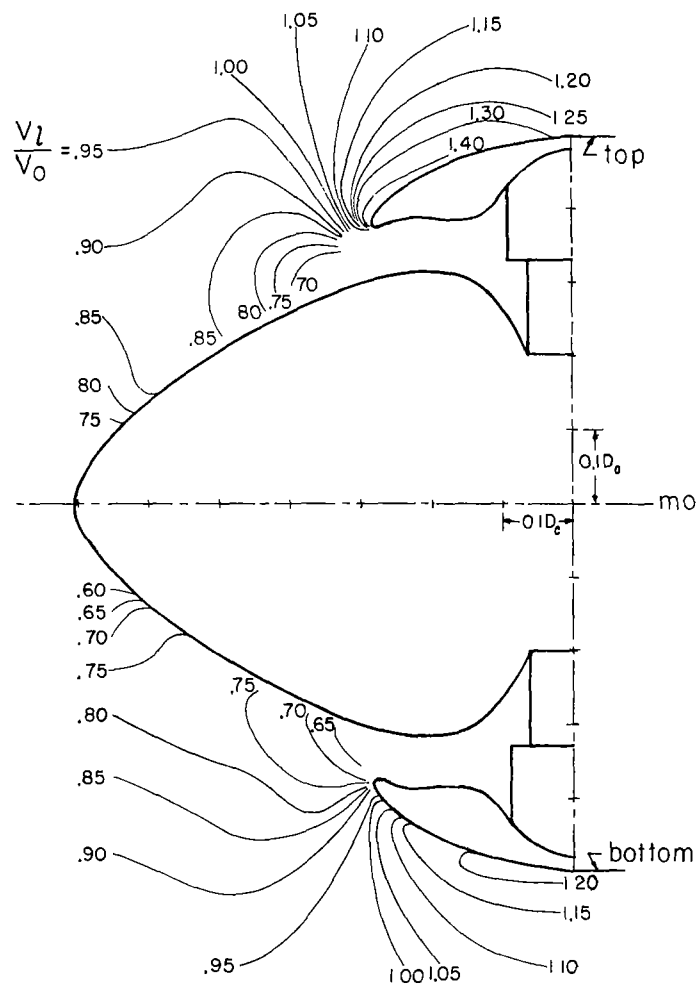


velocity ratio contours  
(a)  $\alpha = 0^\circ$ ,  $\delta = 0^\circ$ ,  $\frac{V_1}{V_0} = 0.23$

lines of constant flow angle

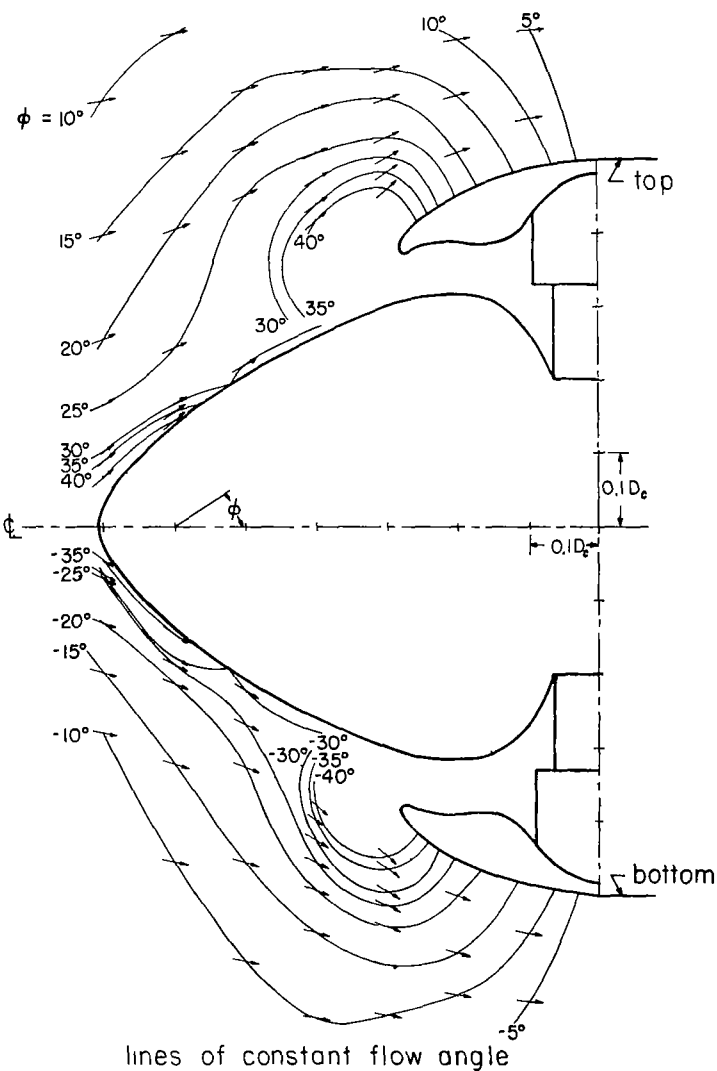
NATIONAL ADVISORY  
COMMITTEE FOR AERONAUTICS

Figure 8.-Velocity and direction of flow in vicinity of spinner and cowling. Propeller removed.



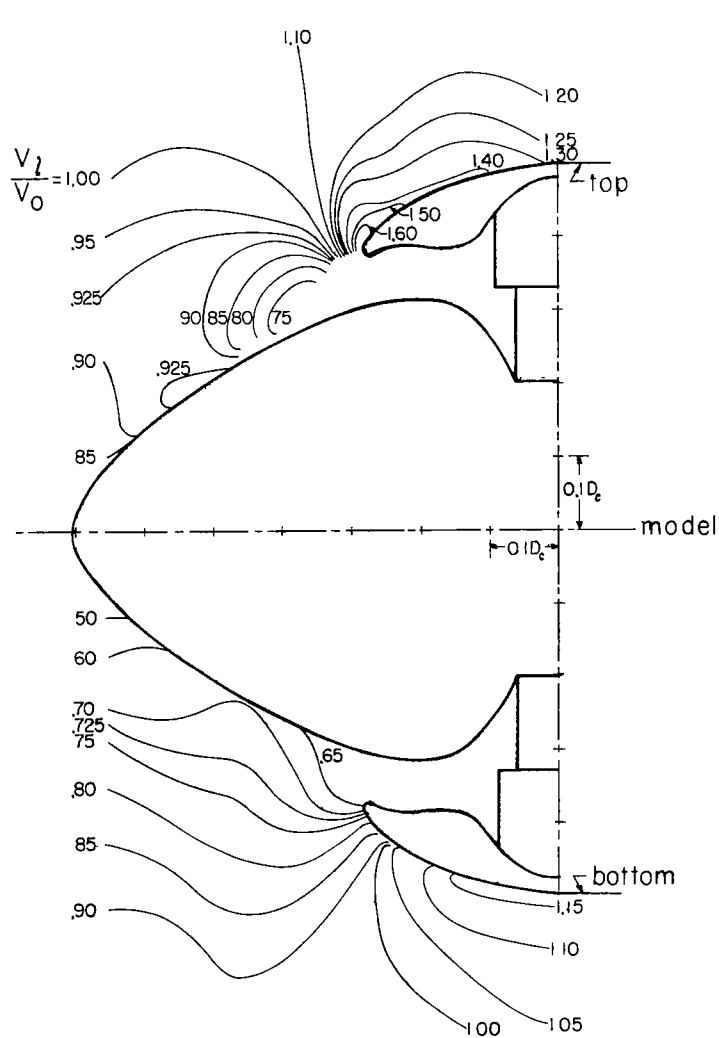
velocity ratio contours  
 (b)  $\alpha = 5^\circ$ ,  $\delta = 0^\circ$ ;  $\frac{V_1}{V_0} = 0.23$

Figure 8. - Continued.



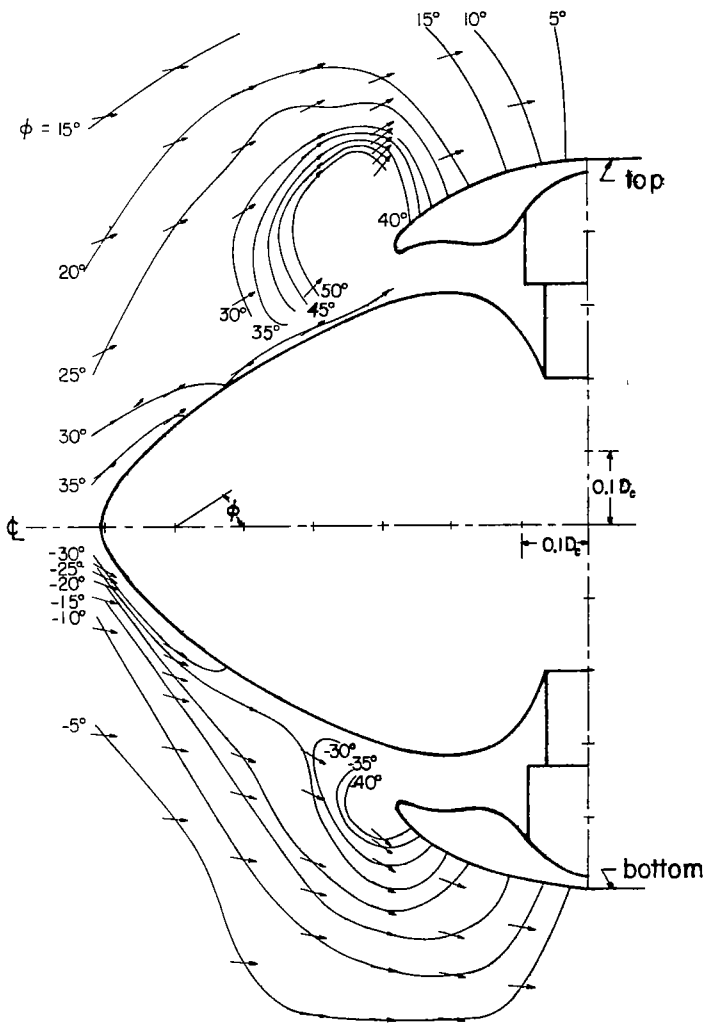
lines of constant flow angle

NATIONAL ADVISORY  
 COMMITTEE FOR AERONAUTICS



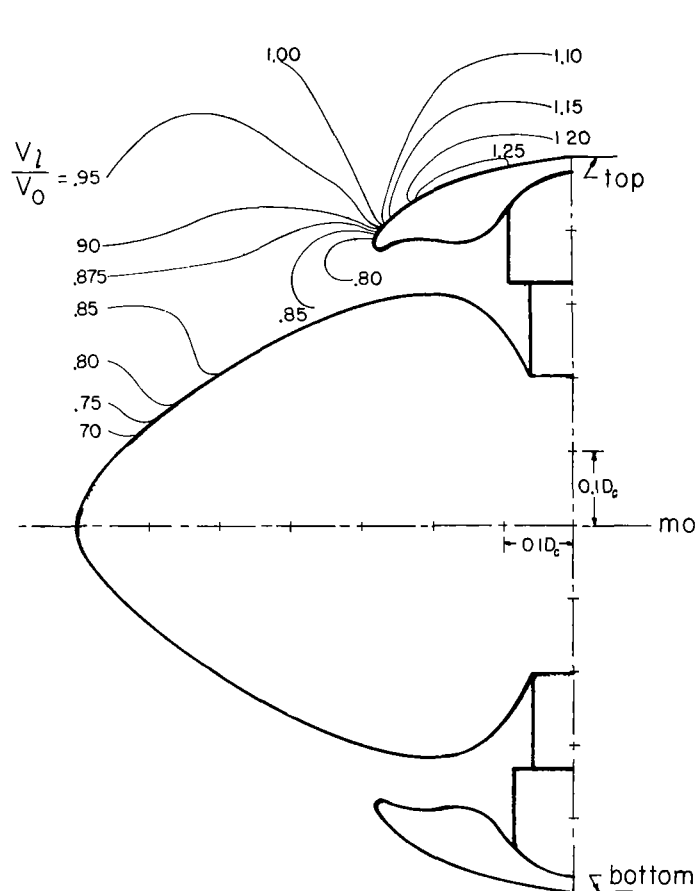
velocity ratio contours  
(c)  $\alpha = 10^\circ$ ,  $\delta = 0^\circ$ ,  $\frac{V_1}{V_0} = 0.23$

Figure 8.- Continued.



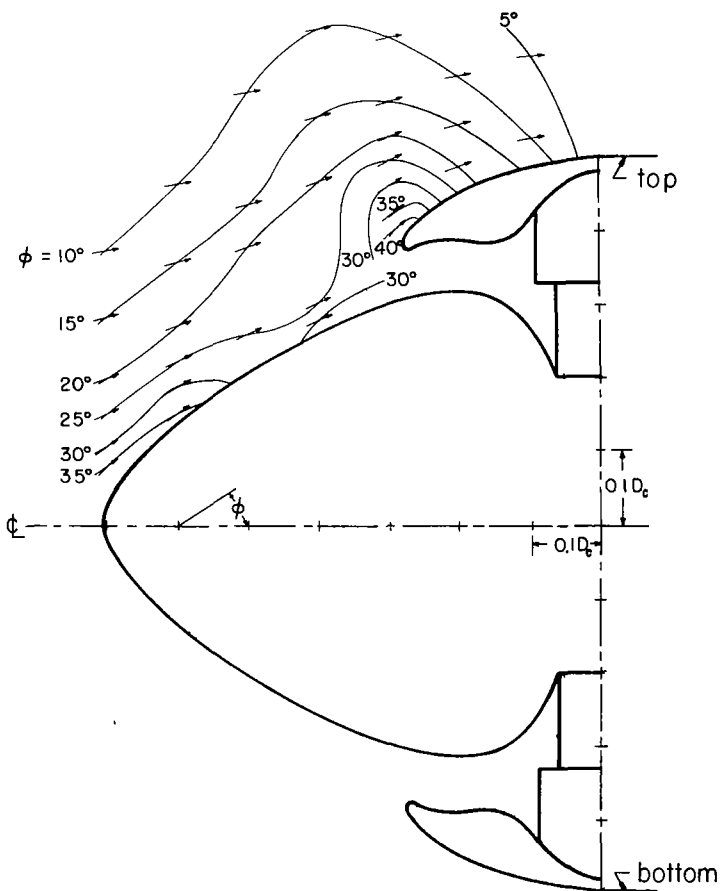
lines of constant flow angle

NATIONAL ADVISORY  
COMMITTEE FOR AERONAUTICS

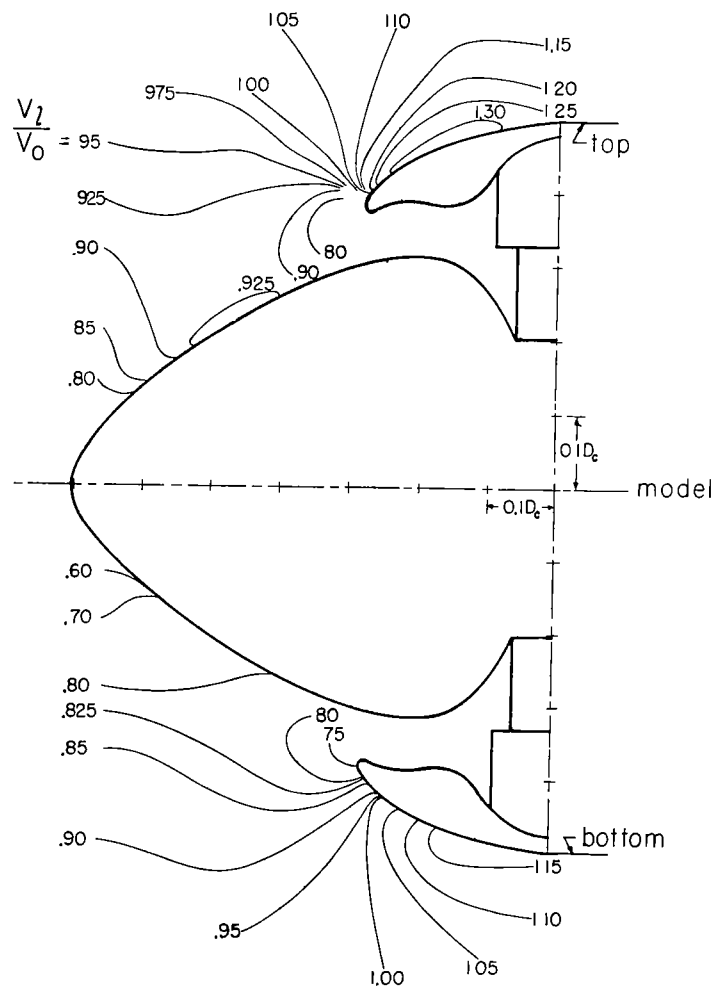


velocity ratio contours  
(d)  $\alpha = 0^\circ$ ,  $\delta = 10^\circ$ ,  $\frac{V_i}{V_0} = 0.70$

Figure 8.- Continued.

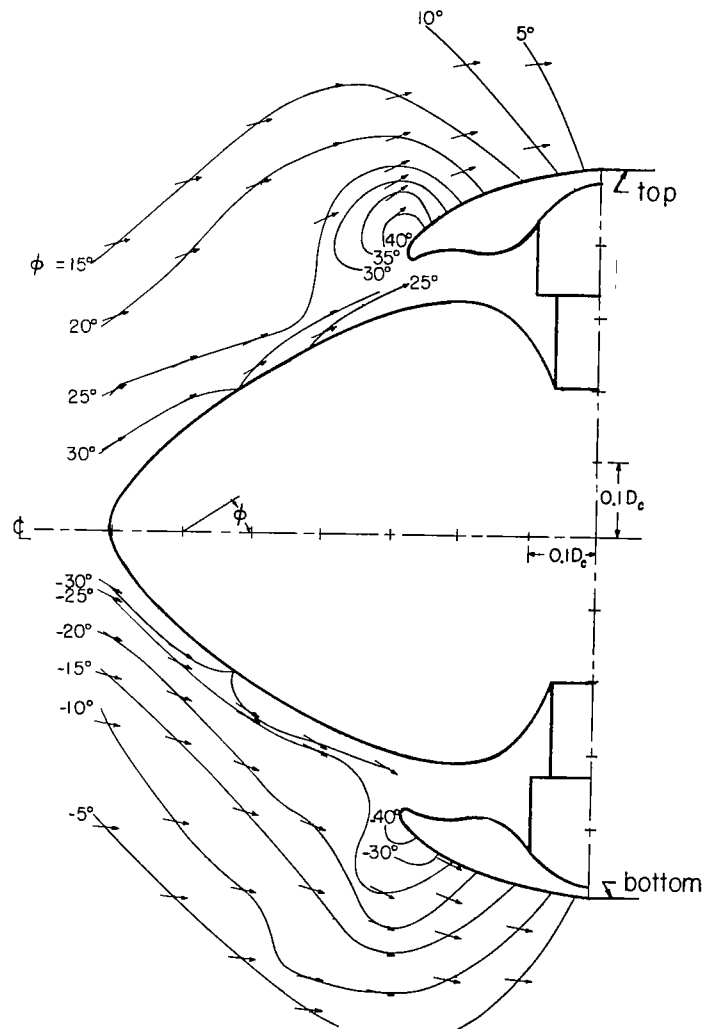


lines of constant flow angle



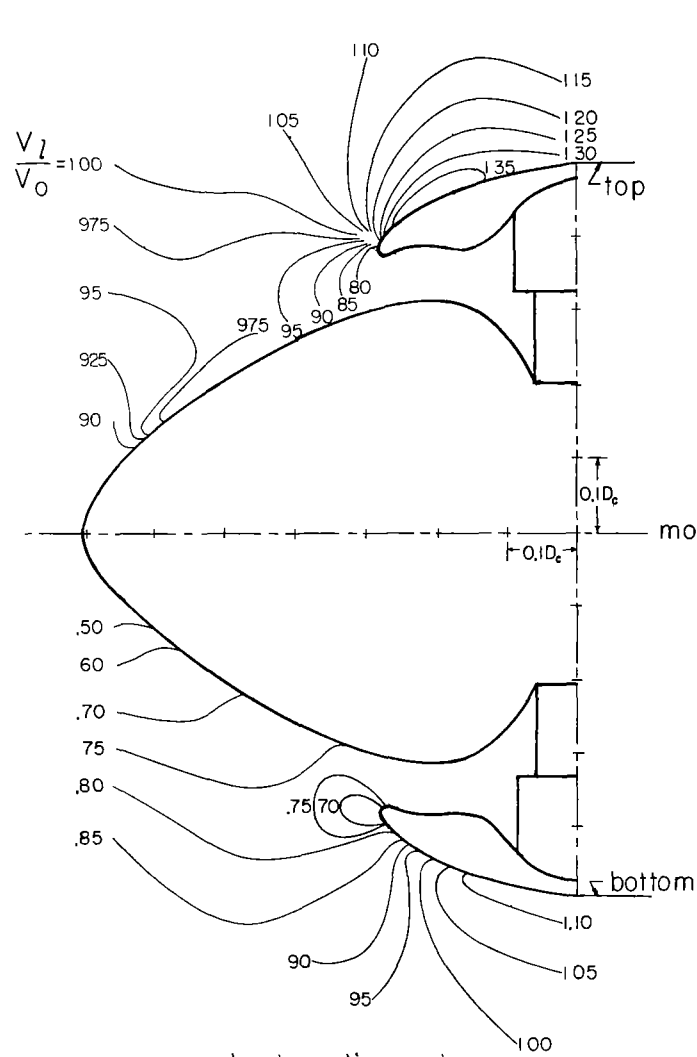
velocity ratio contours  
(e)  $\alpha = 5^\circ$ ,  $\delta = 10^\circ$ ,  $\frac{V_1}{V_0} = 0.69$

Figure 8.- Continued.



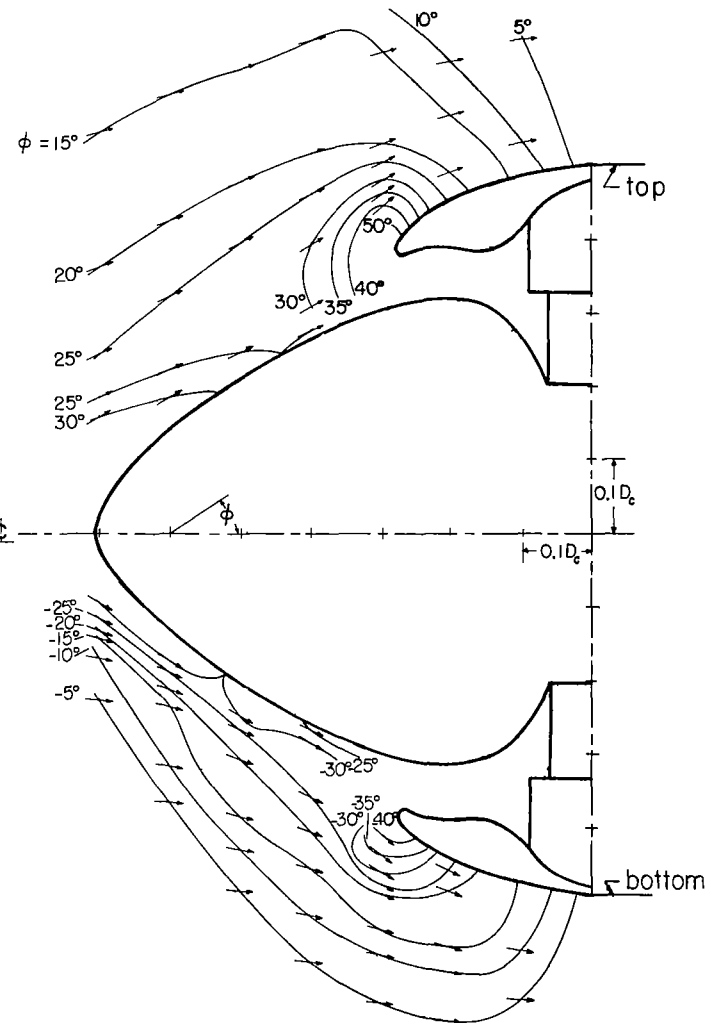
lines of constant flow angle

NATIONAL ADVISORY  
COMMITTEE FOR AERONAUTICS

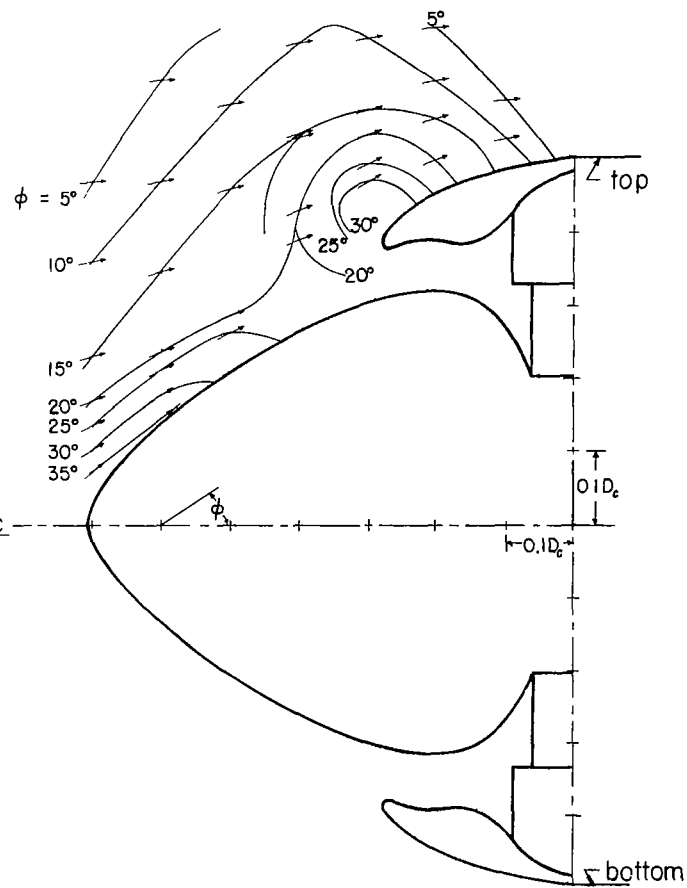
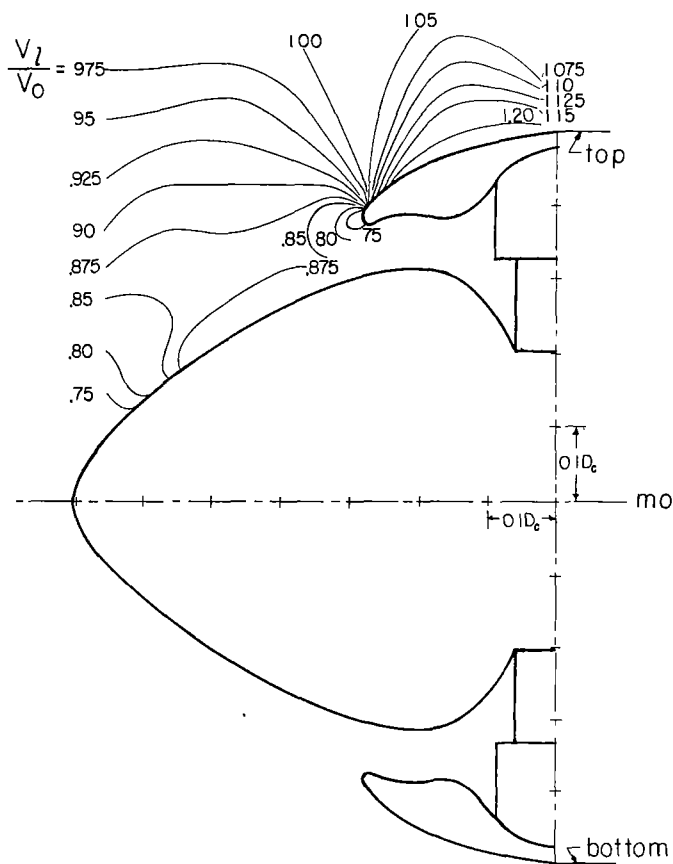


velocity ratio contours  
(f)  $\alpha = 10^\circ$ ,  $\delta = 10^\circ$ ,  $\frac{V_l}{V_0} = 0.66$

Figure 8.- Continued.



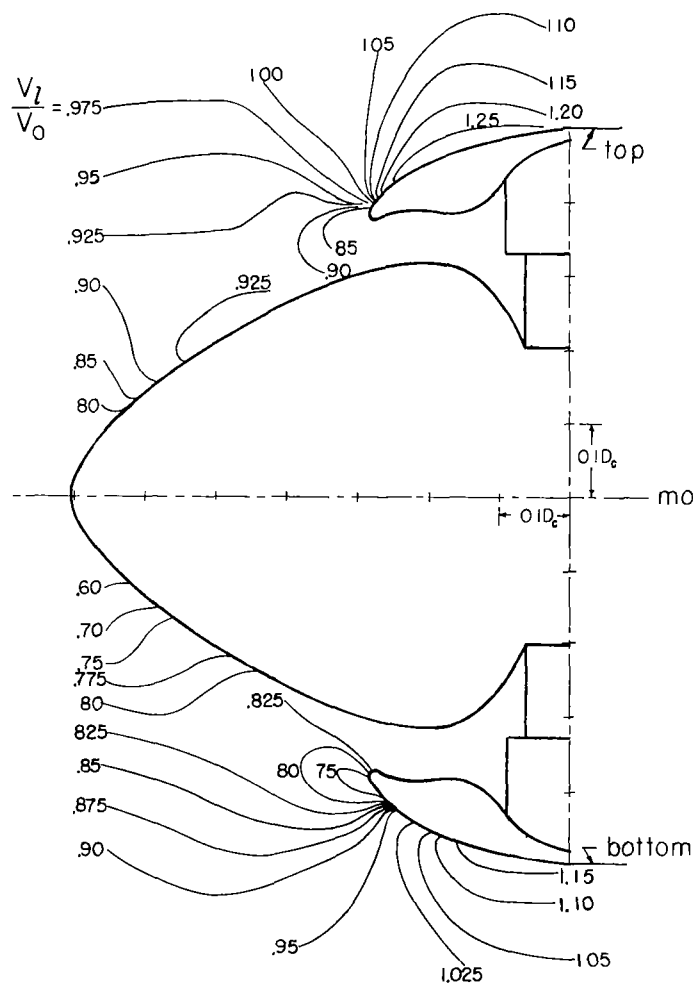
lines of constant flow angle



velocity ratio contours  
 (g)  $\alpha = 0^\circ$ ,  $\delta = 20^\circ$ ,  $\frac{V_1}{V_0} = 0.86$   
 Figure 8.- Continued.

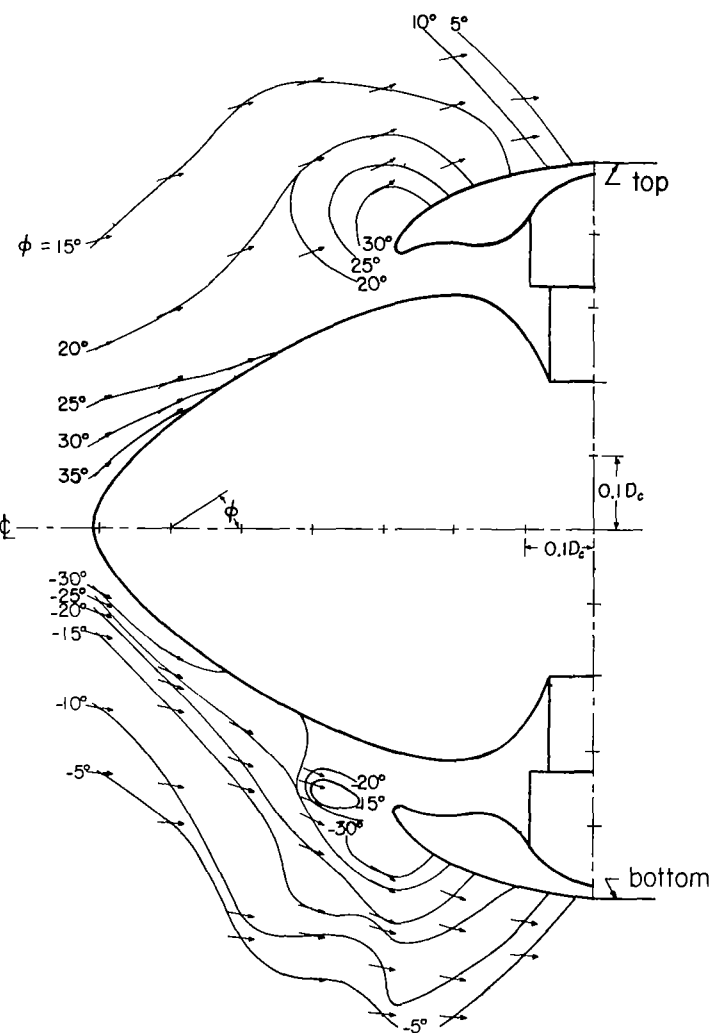
lines of constant flow angle

NATIONAL ADVISORY  
 COMMITTEE FOR AERONAUTICS



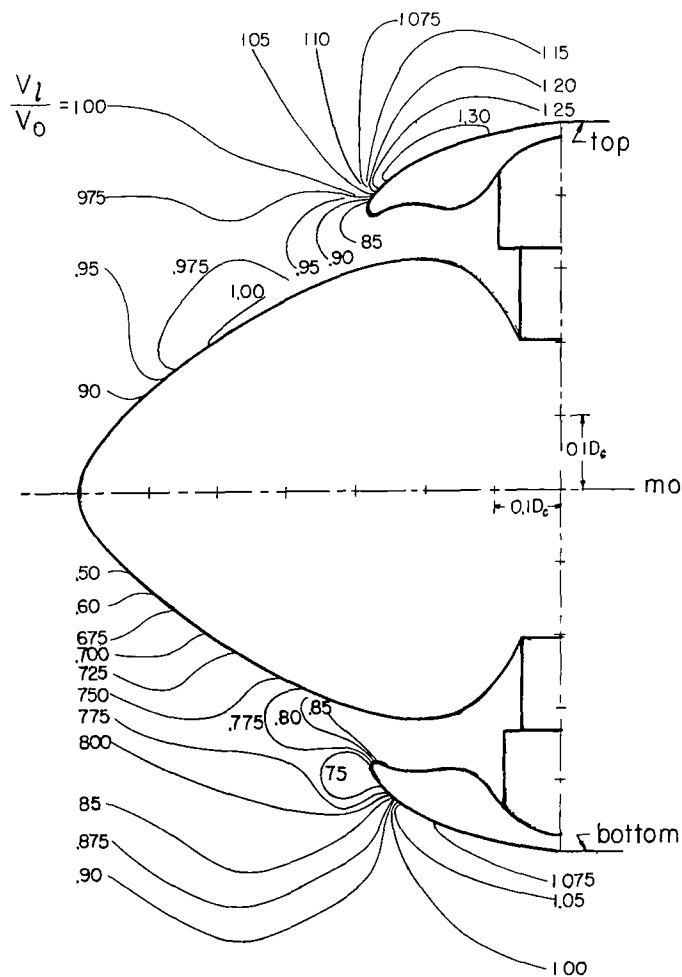
velocity ratio contours  
(h)  $\alpha = 5^\circ$ ,  $\delta = 20^\circ$ ,  $\frac{V_i}{V_0} = 0.85$

Figure 8.- Continued.



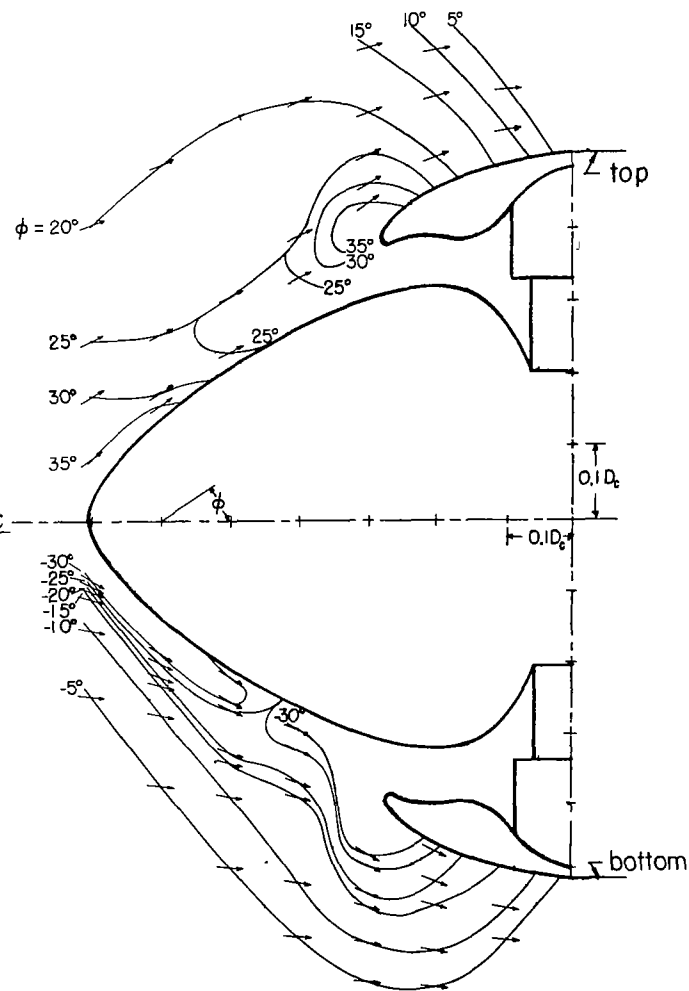
lines of constant flow angle

NATIONAL ADVISORY  
COMMITTEE FOR AERONAUTICS



velocity ratio contours  
(i)  $\alpha = 10^\circ$ ,  $\delta = 20^\circ$ ,  $\frac{V_i}{V_0} = 0.81$

Figure 8.- Concluded.



lines of constant flow angle

NATIONAL ADVISORY  
COMMITTEE FOR AERONAUTICS

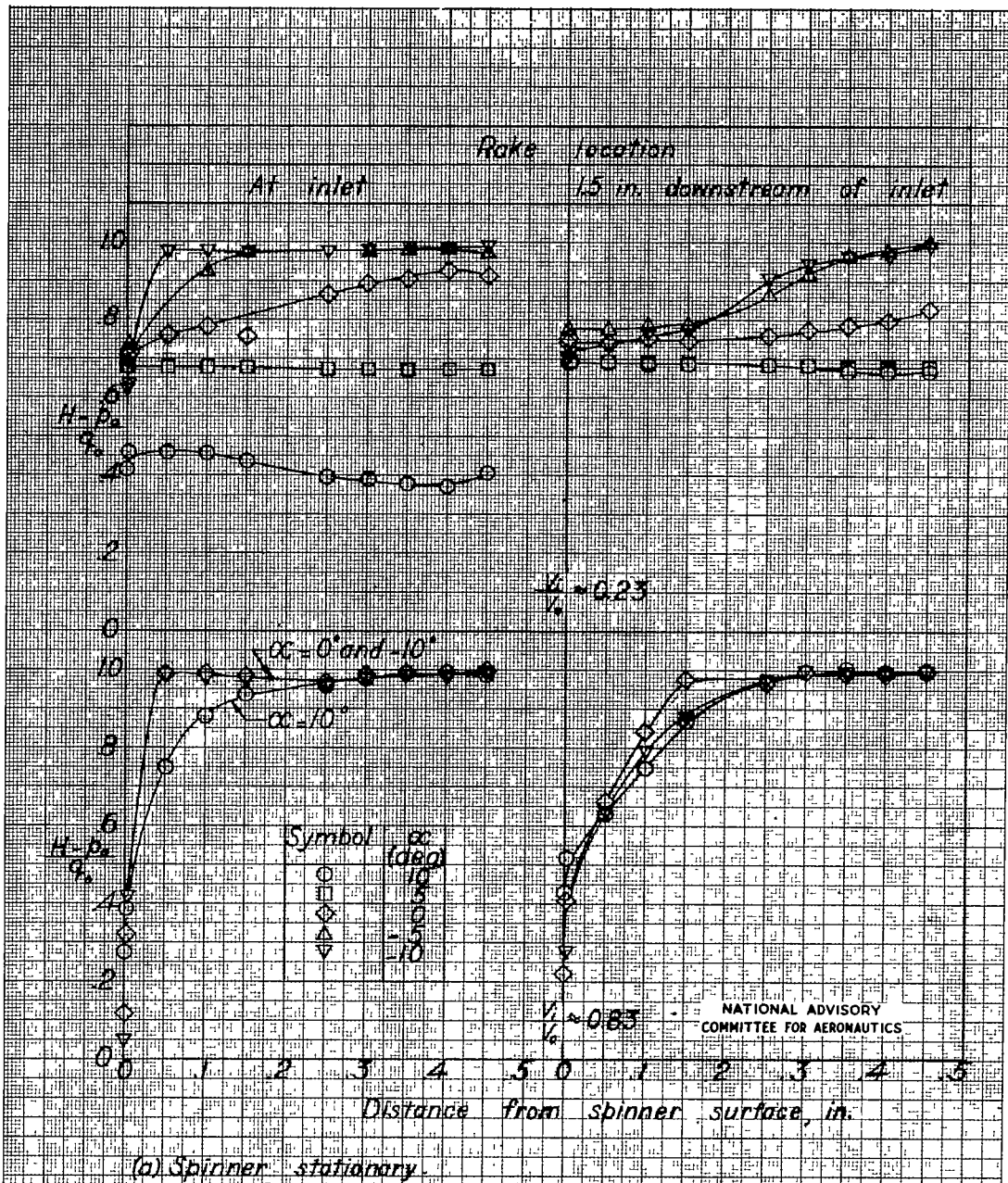


Figure 9 - Total-pressure recovery ratio distribution in boundary layer of spinner at top of inlet. Propeller removed.

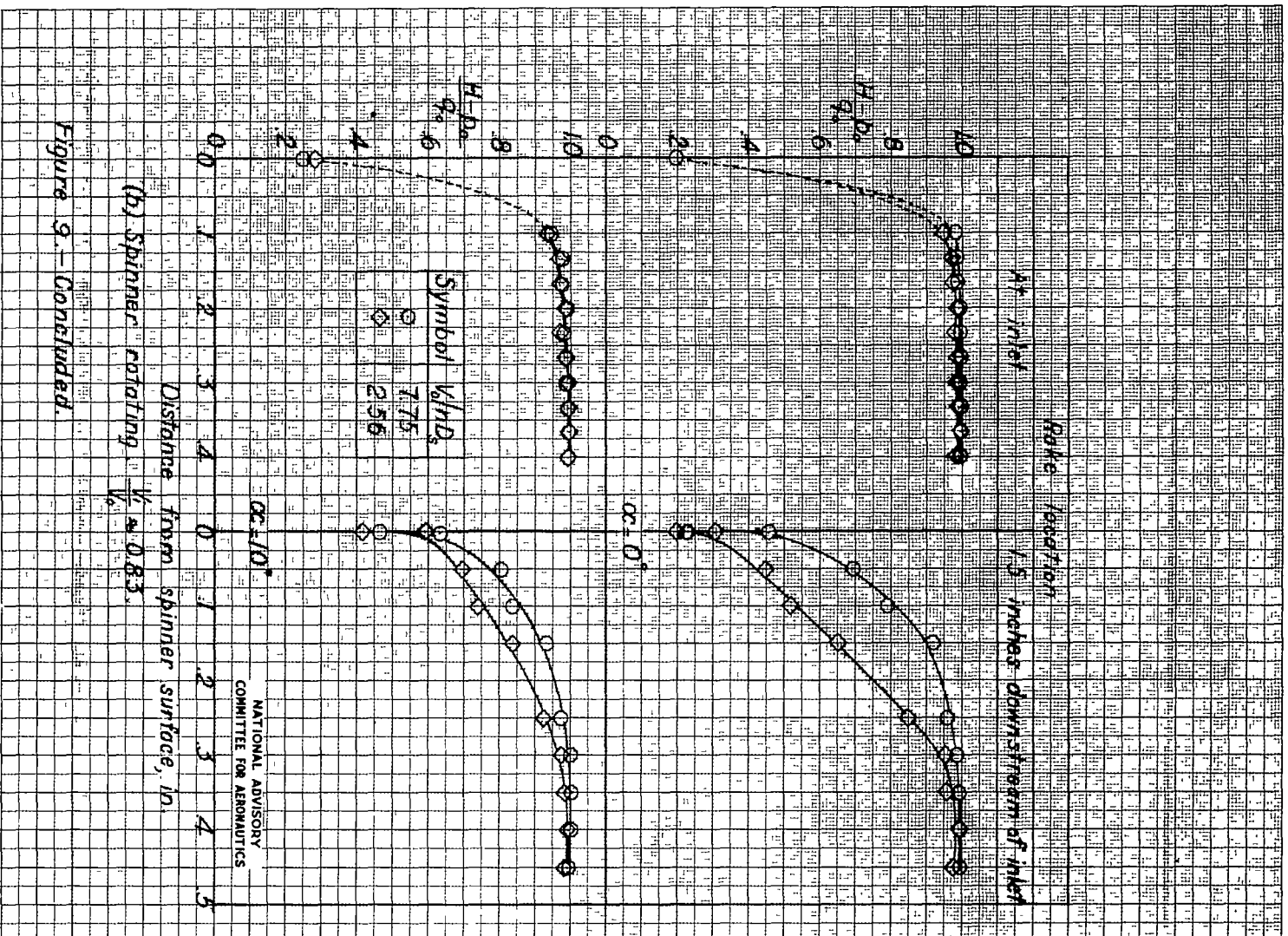


Figure 9.—Continued.

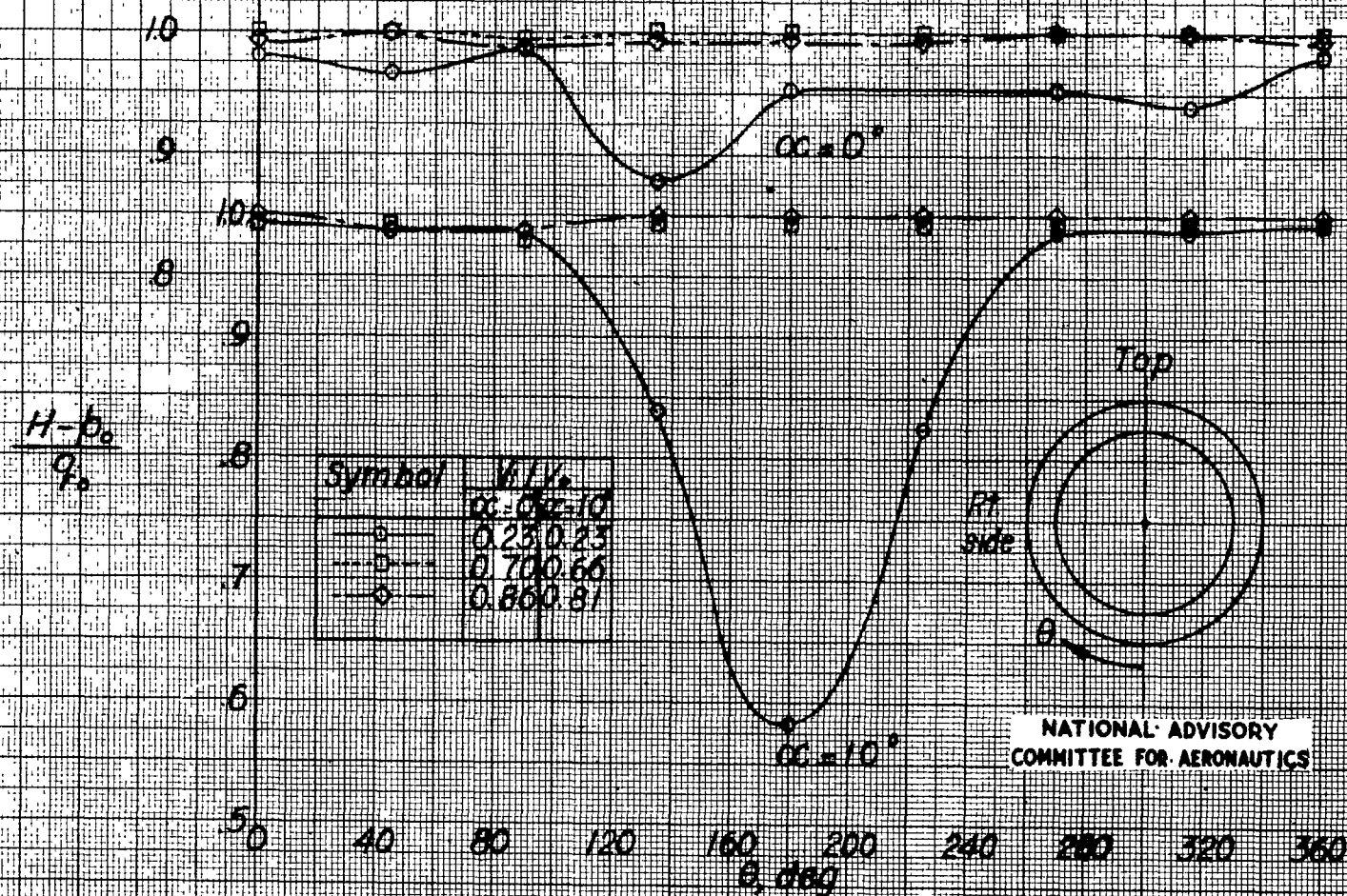
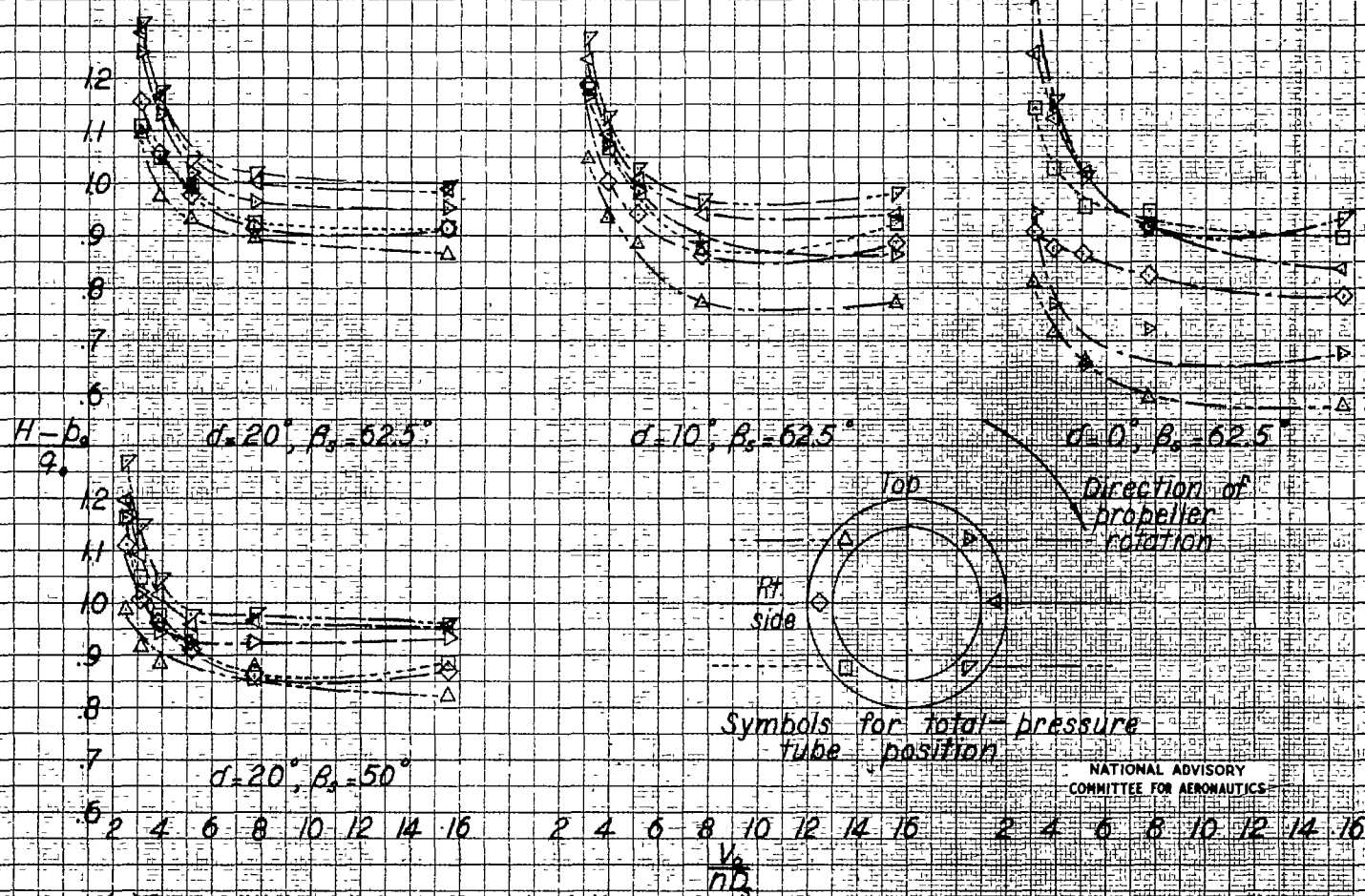
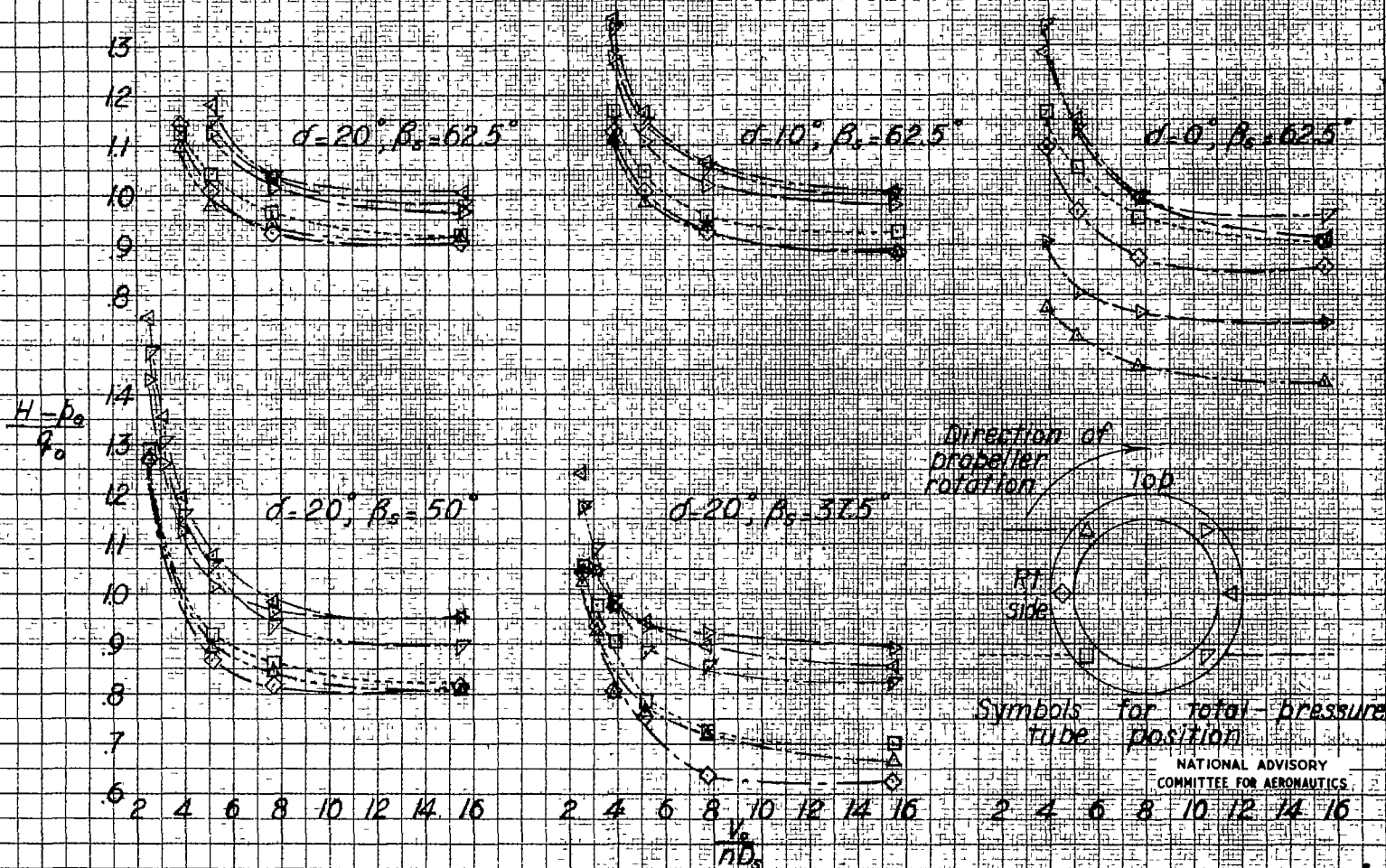


Figure 10—Circumferential variation of total-pressure recovery ratio at inlet for propeller-removed test condition.



(a) Oval-shanked propeller installed.

Figure 11 - Total-pressure recovery ratio at inlet for several circumferential positions for propeller-installed test conditions  $\alpha = 10^\circ$ .



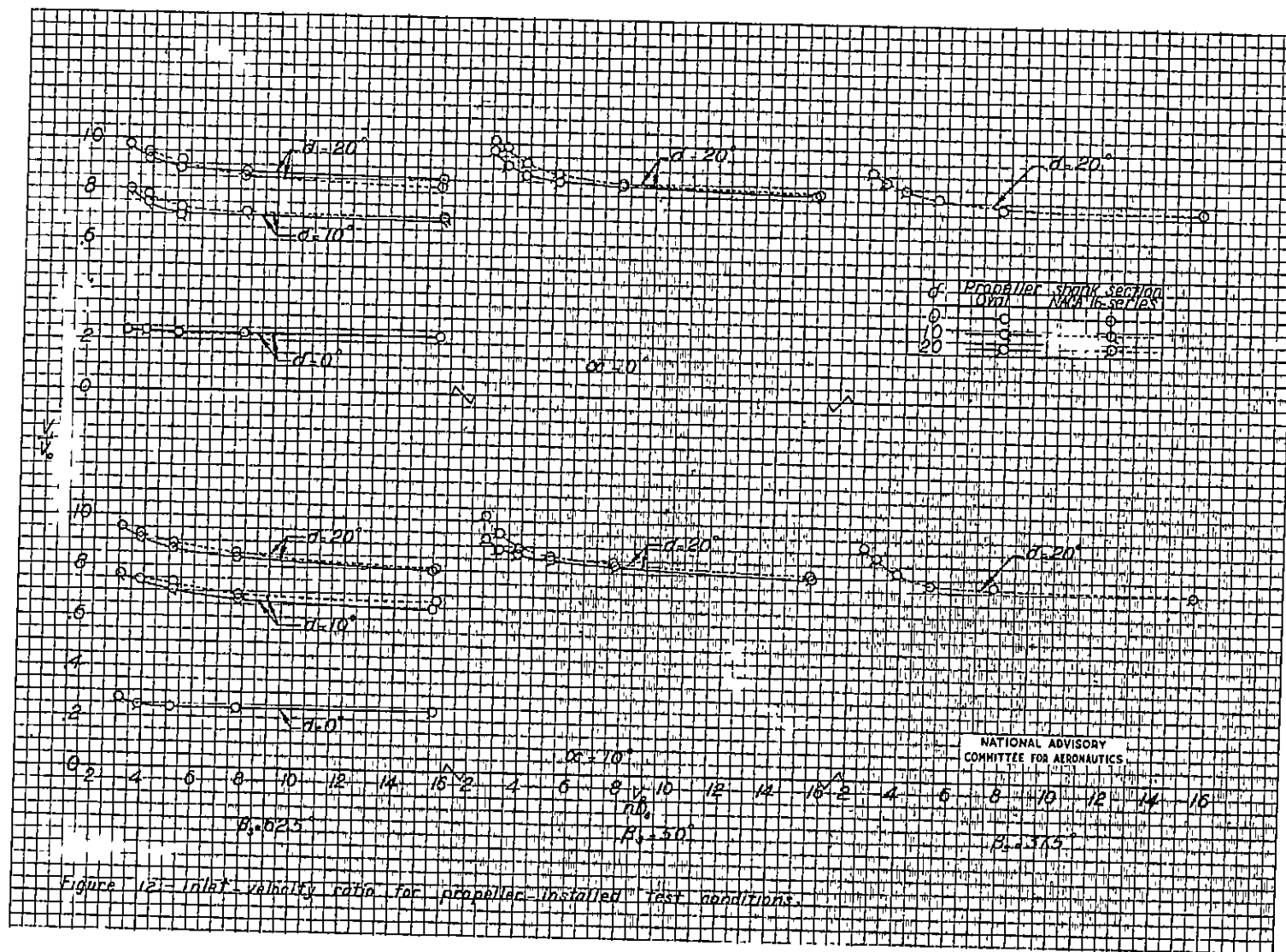


Figure 12 - Inlet velocity ratio for propeller installed test conditions.

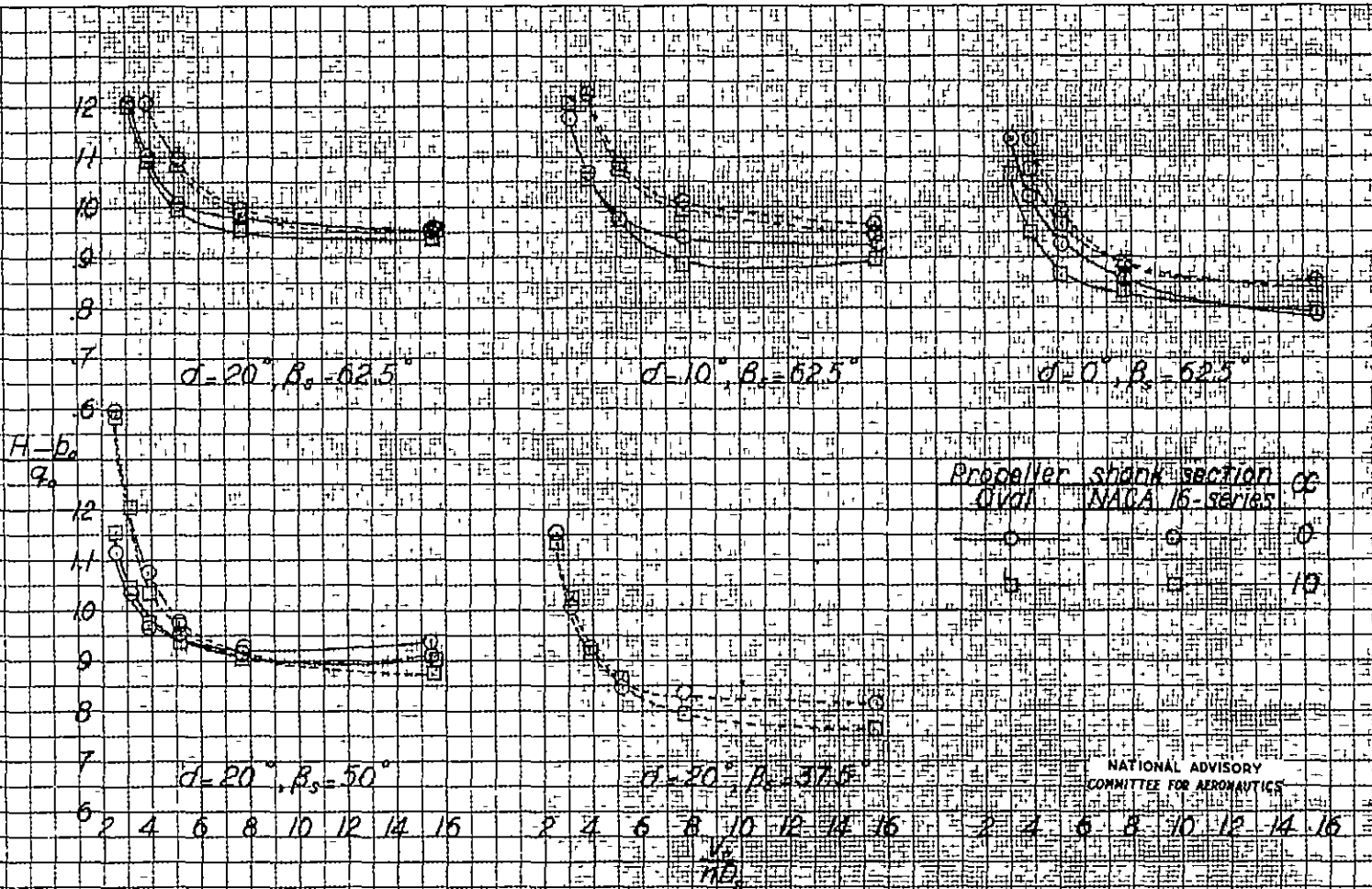
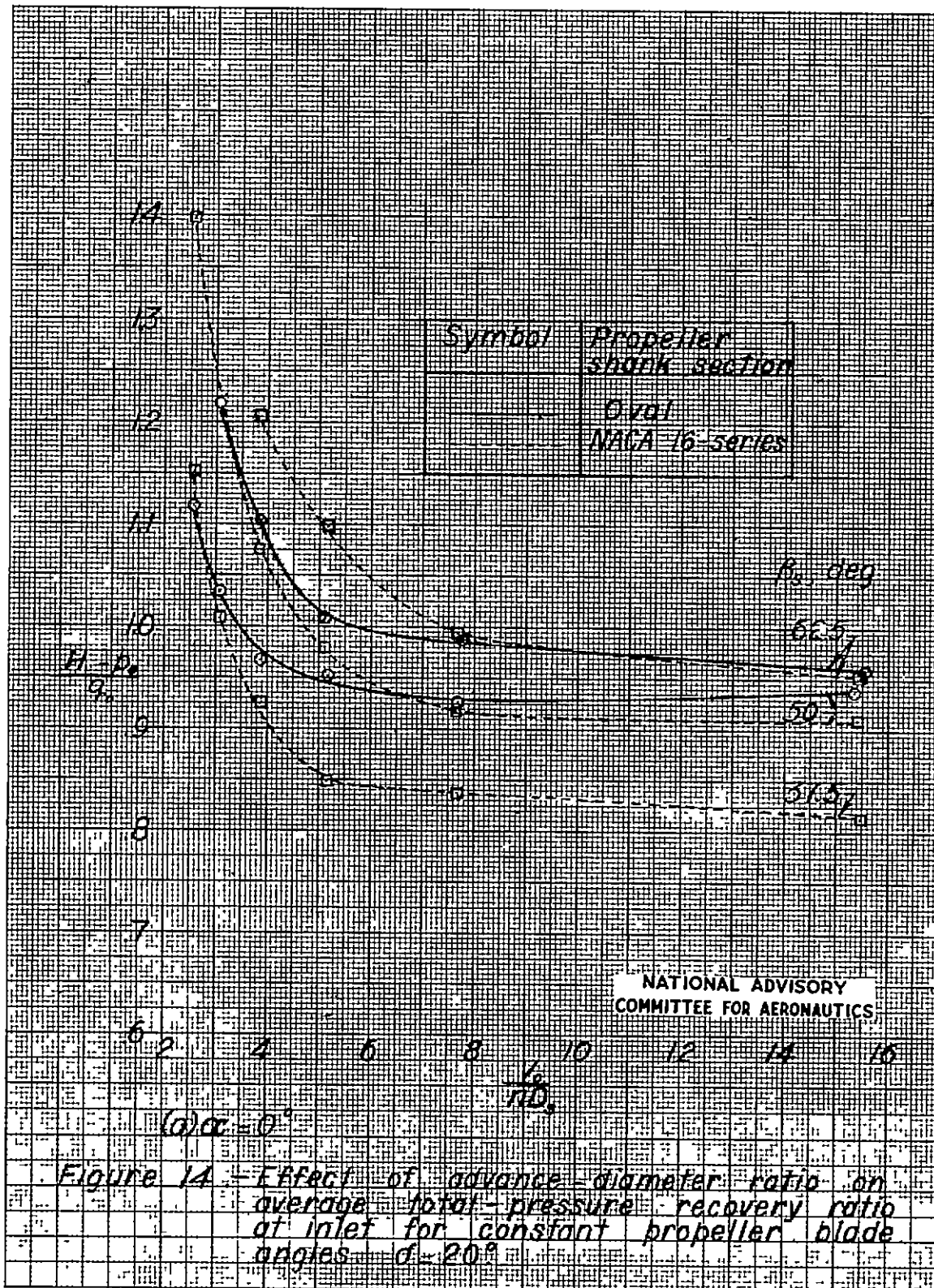
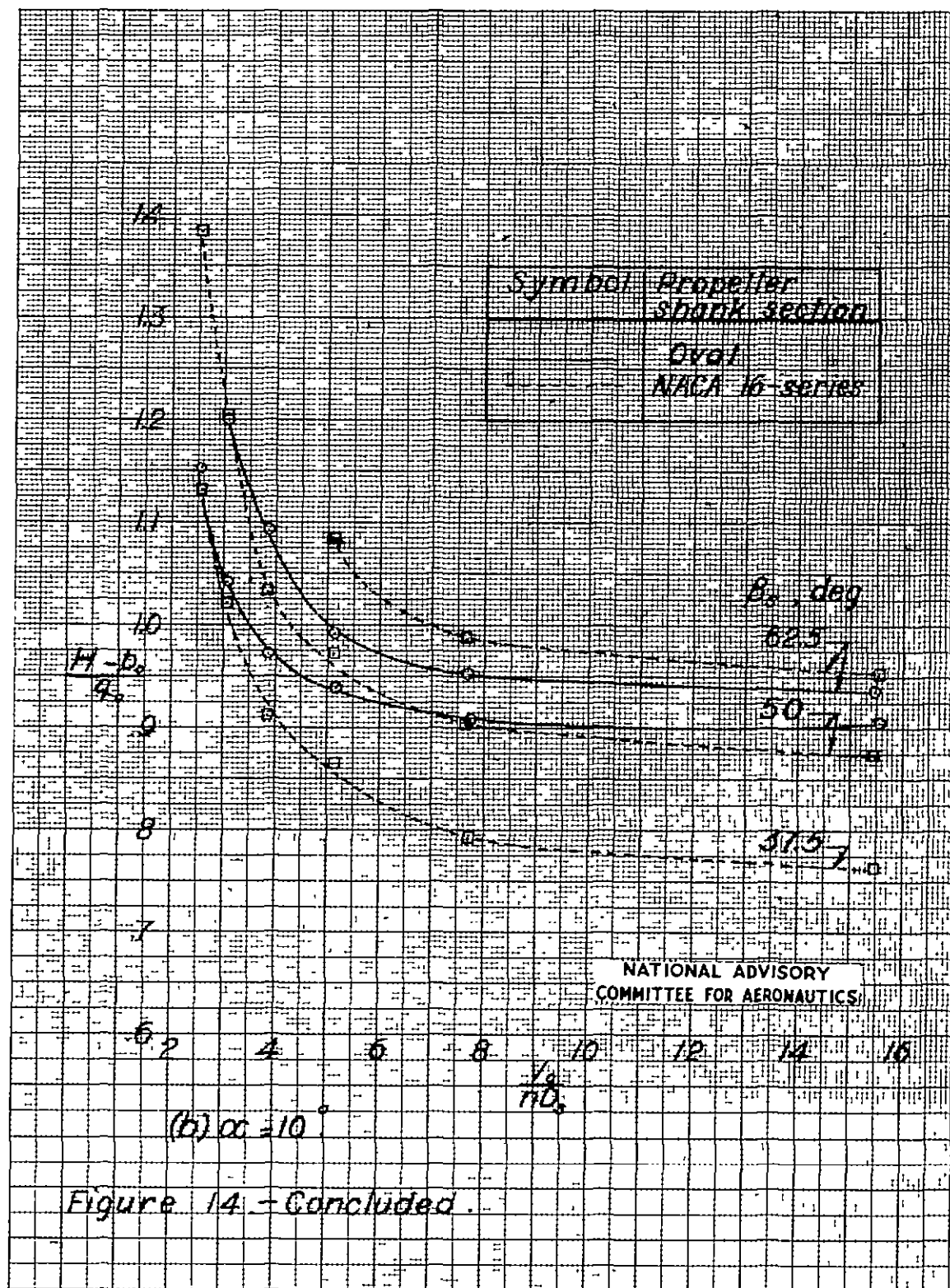
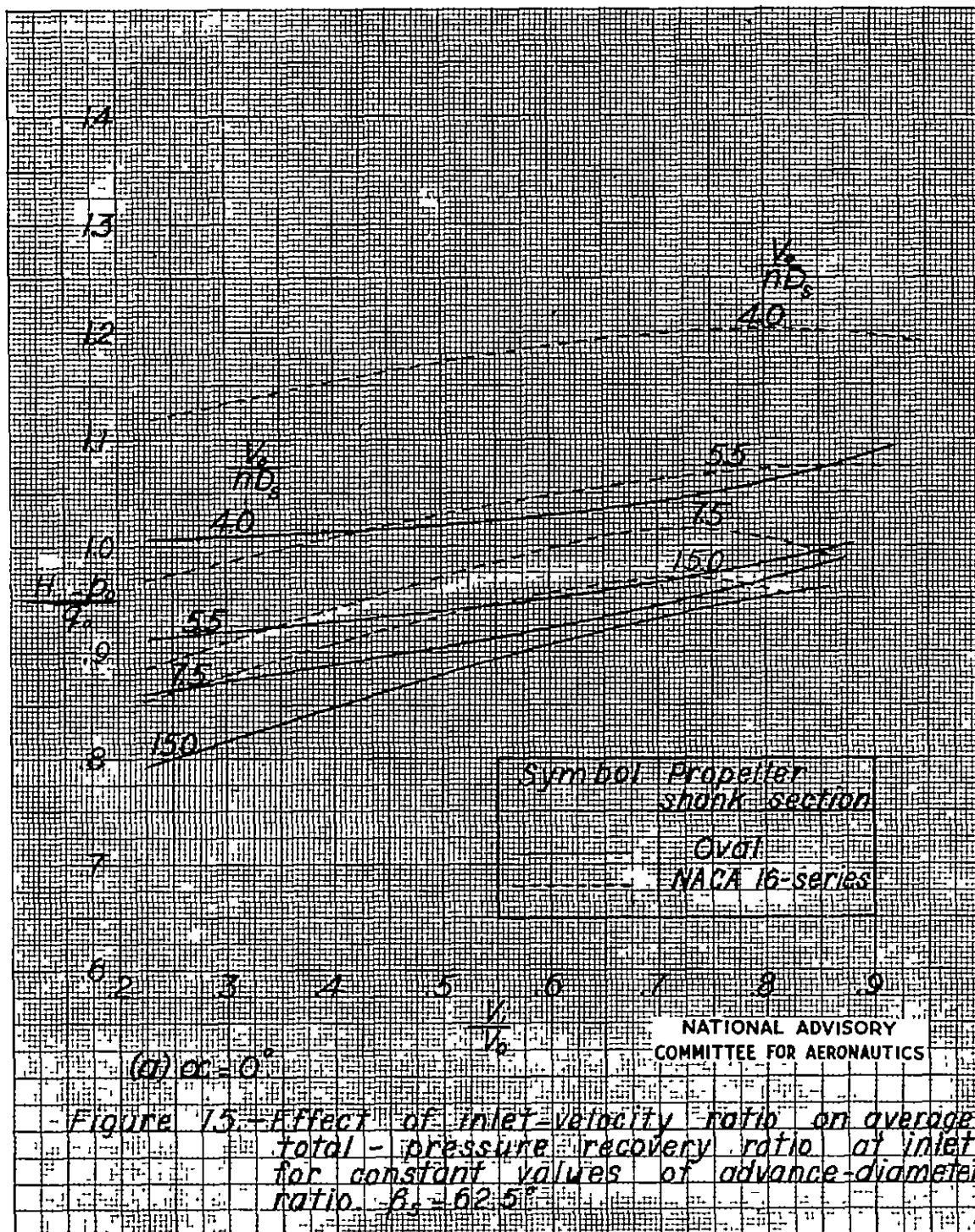
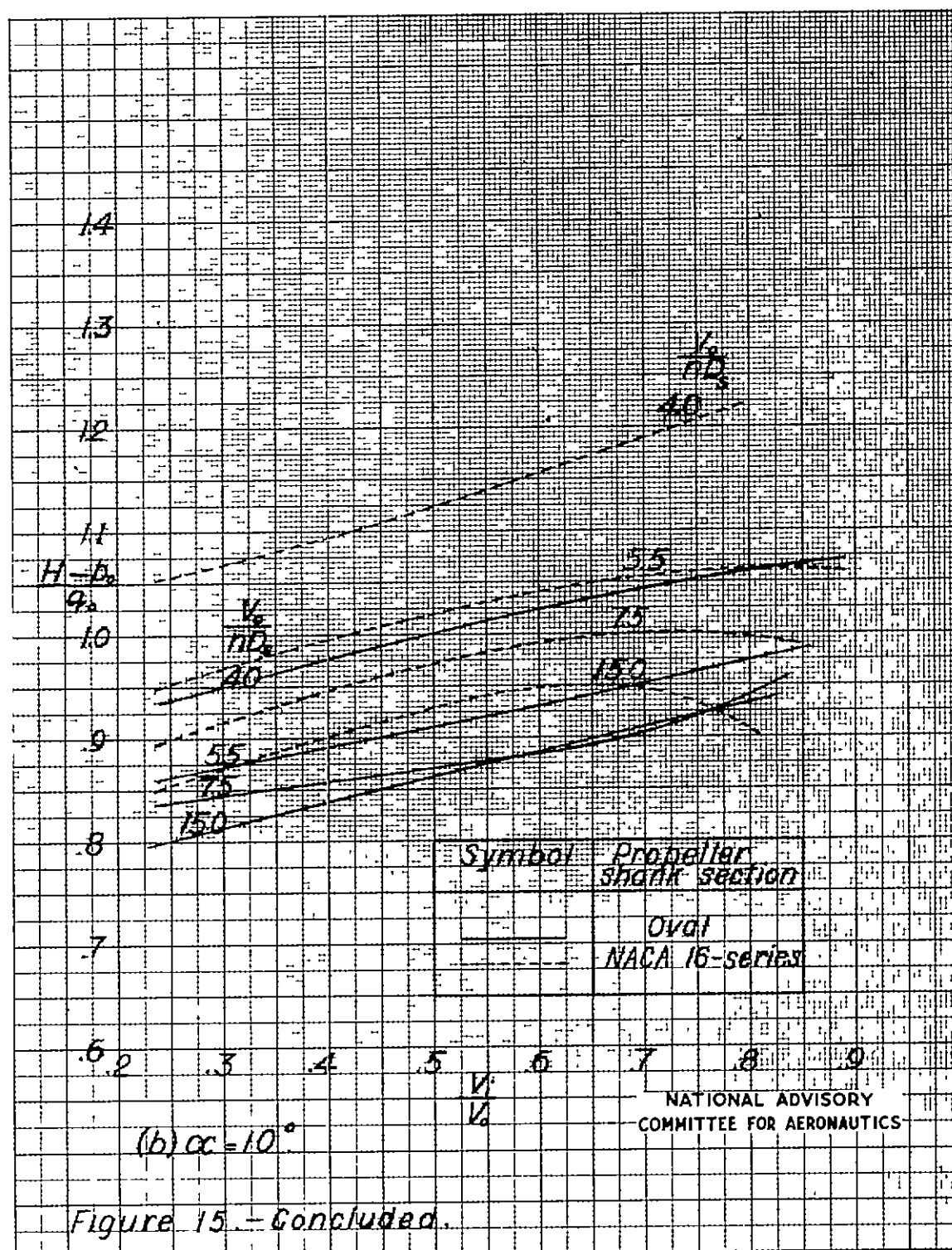


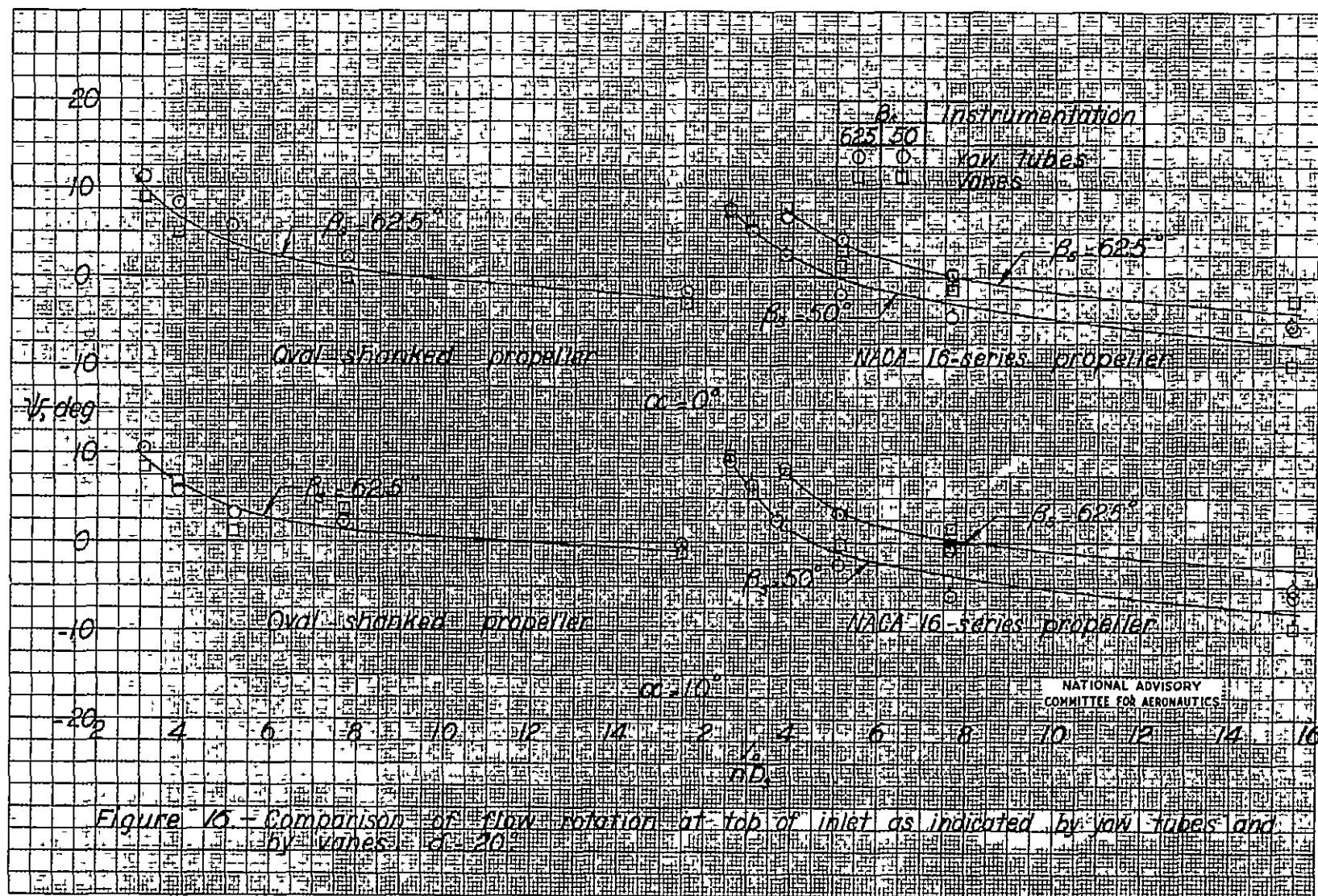
Figure 13.- Average total-pressure recovery ratio in inlet for propeller-installed test conditions.











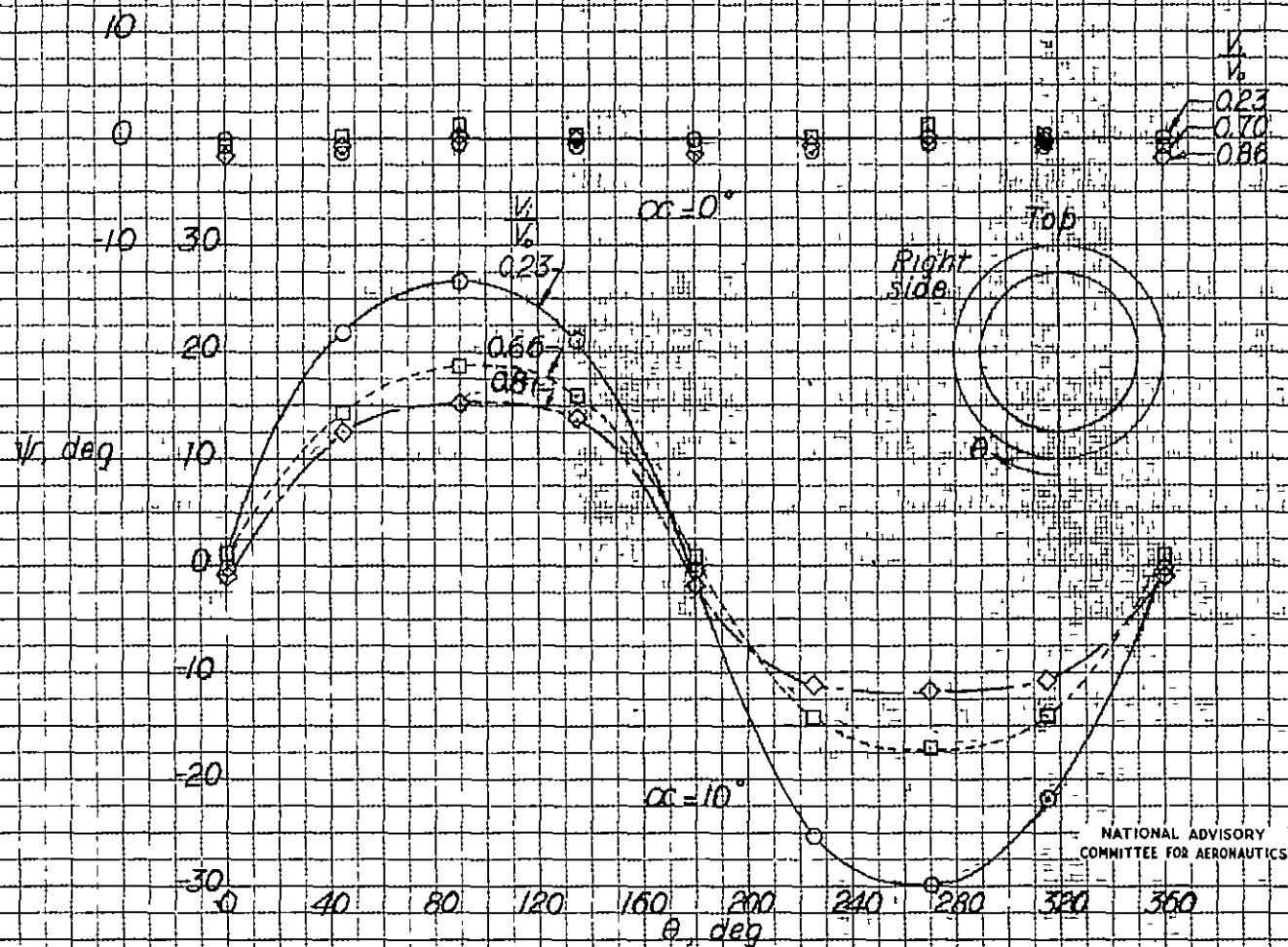
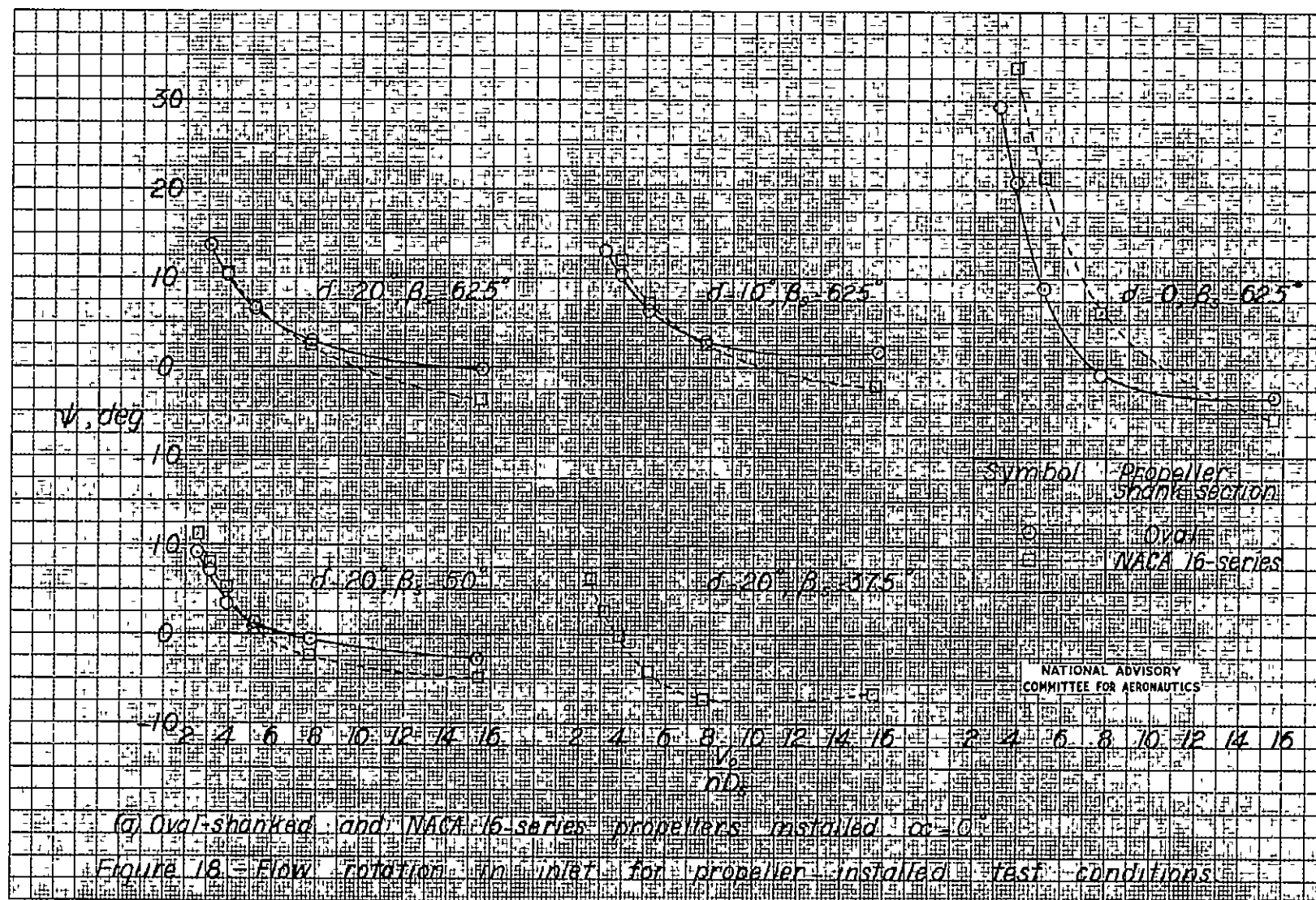
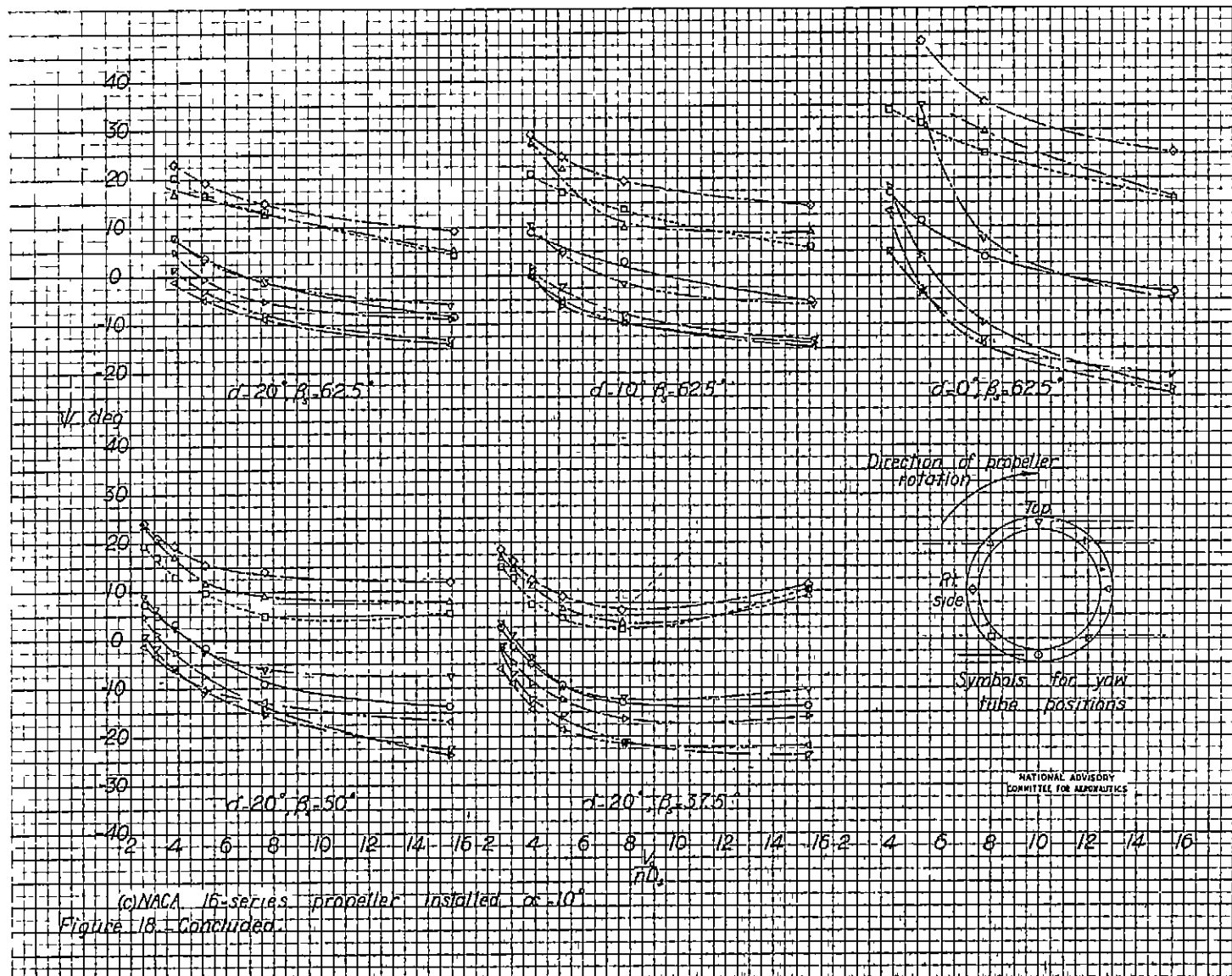


Figure 17. - Circumferential variation of flow rotation in inlet for propeller-removed test condition





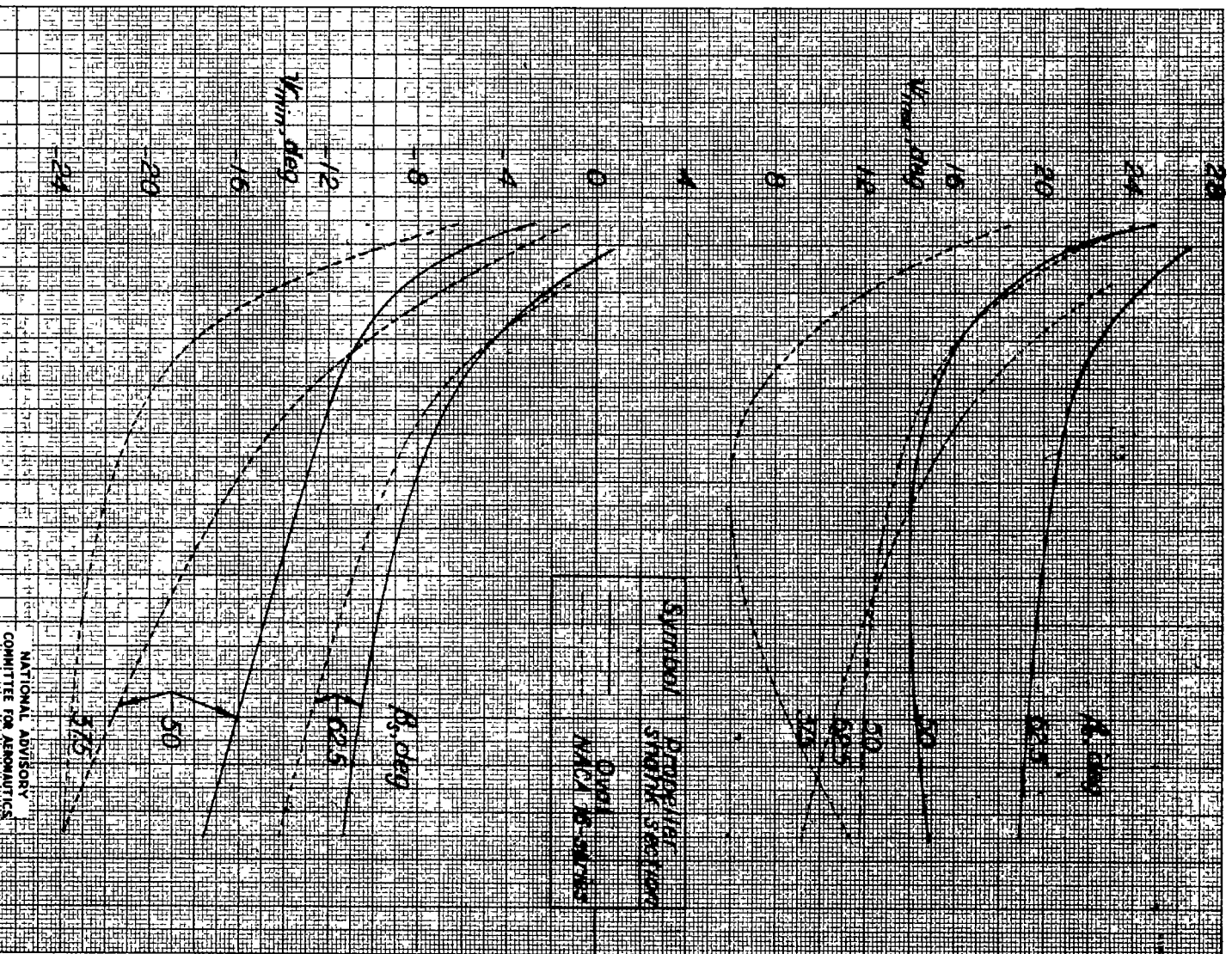


Figure 19 - Concluded

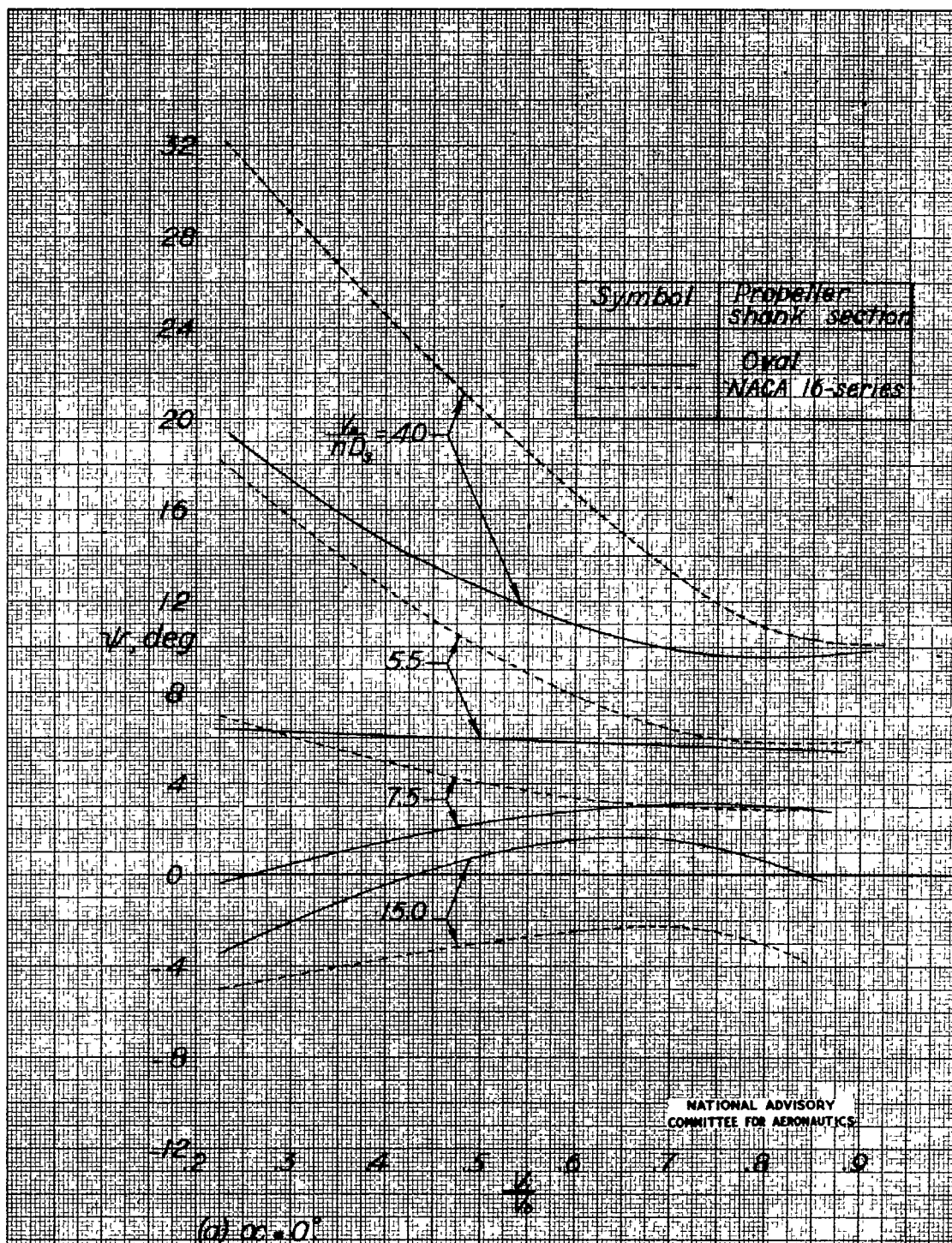
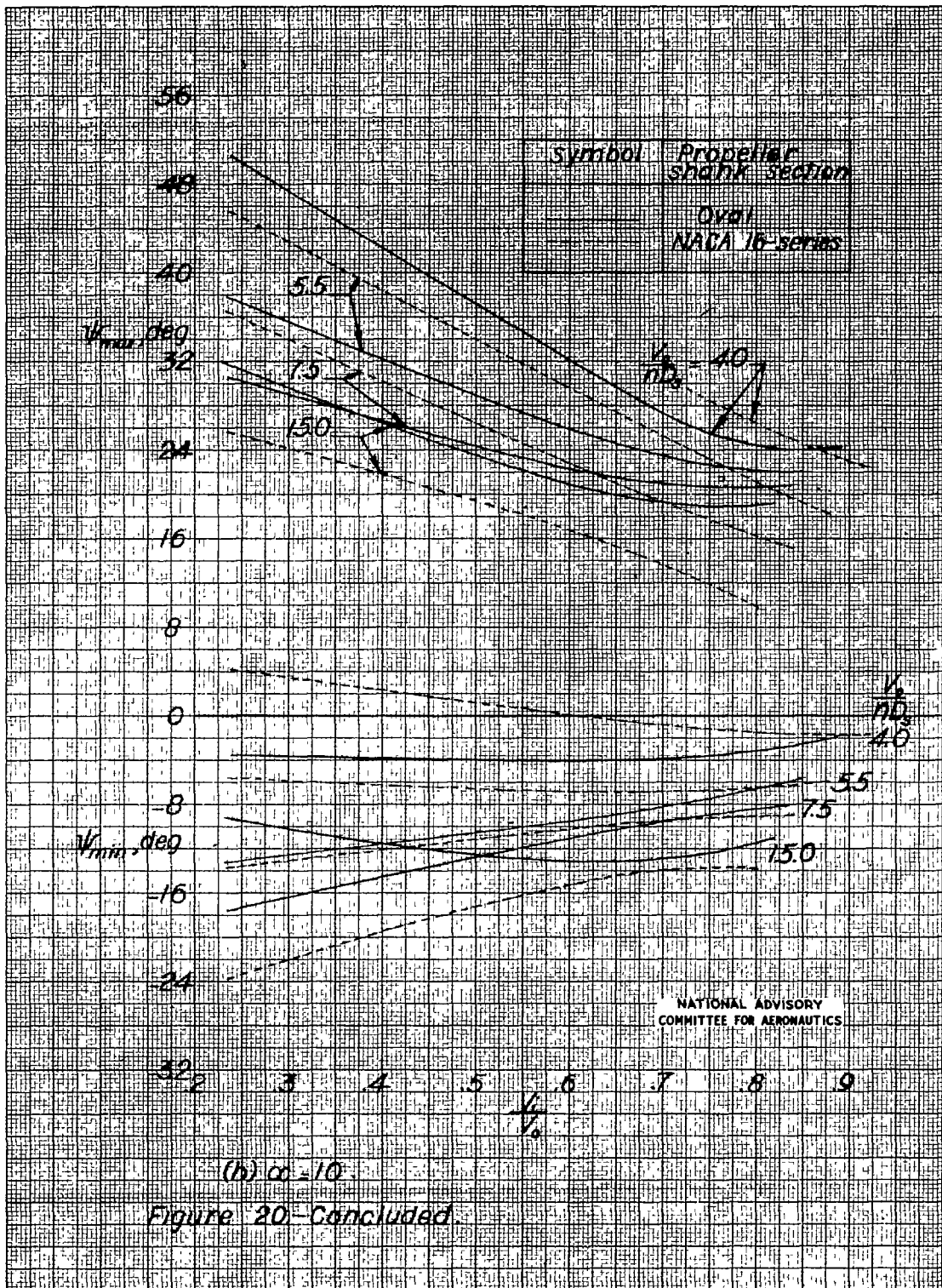


Figure 20.—Effect of inlet velocity ratio on flow rotation in inlet at constant values of advance-diameter ratio  $\beta_0 = 62.5^\circ$





3 1176 01403 6041

**DO NOT REMOVE SLIP FROM MATERIAL**

Delete your name from this slip when returning material to the library.

NAME	MS